2015

Structural dynamics of E. coli single-stranded DNA binding protein reveal DNA wrapping and unwrapping pathways

Sukrit Suksombat
University of Illinois at Urbana-Champaign

Rustem Khafizov
University of Illinois at Urbana-Champaign

Alexander G. Kozlov
Washington University School of Medicine in St. Louis

Timothy M. Lohman
Washington University School of Medicine in St. Louis

Yann R. Chemla
University of Illinois at Urbana-Champaign

Structural dynamics of *E. coli* single-stranded DNA binding protein reveal DNA wrapping and unwrapping pathways

Sukrit Suksombat, Rustem Khafizov, Alexander G Kozlov, Timothy M Lohman, Yann R Chemla

DOI: http://dx.doi.org/10.7554/eLife.08193

Cite as: eLife 2015;10.7554/eLife.08193

Received: 21 April 2015
Accepted: 24 August 2015
Published: 25 August 2015

Structural dynamics of *E. coli* single-stranded DNA binding protein reveal DNA wrapping and unwrapping pathways

Sukrit Suksombat[1], Rustem Khafizov[1], Alexander G. Kozlov[2],

Timothy M. Lohman[2]*, and Yann R. Chemla[1]*

Affiliations:

[1]Department of Physics, Center for the Physics of Living Cells, and Center for Biophysics and Computational Biology, University of Illinois at Urbana-Champaign, Urbana, Illinois, USA.

[2]Department of Biochemistry and Molecular Biophysics, Washington University School of Medicine, St. Louis, Missouri, USA.

*Correspondence to: ychemla@illinois.edu and lohman@biochem.wustl.edu

ABSTRACT

Escherichia coli single-stranded (ss)DNA binding (SSB) protein mediates genome maintenance processes by regulating access to ssDNA. This homotetrameric protein wraps ssDNA in multiple distinct binding modes that may be used selectively in different DNA processes, and whose detailed wrapping topologies remain speculative. Here, we used single-molecule force and fluorescence spectroscopy to investigate *E. coli* SSB binding to ssDNA. Stretching a single ssDNA-SSB complex reveals discrete states that correlate with known binding modes, the likely ssDNA conformations and diffusion dynamics in each, and the kinetic pathways by which the protein wraps ssDNA and is dissociated. The data allow us to construct an energy landscape for the ssDNA-SSB complex, revealing that unwrapping energy costs increase the more ssDNA is unraveled. Our findings provide insights into the mechanism by which proteins gain access to ssDNA bound by SSB, as demonstrated by experiments in which SSB is displaced by the *E. coli* recombinase RecA.

INTRODUCTION

E. coli Single-Stranded DNA Binding protein (*Eco*SSB) is an essential protein involved in most aspects of genome maintenance [1-3]. It binds with high affinity and little sequence specificity [3][4] to single stranded (ss)DNA intermediates formed during DNA replication, recombination, and repair, protecting them from both nucleolytic and chemical damage. SSB also interacts directly with more than a dozen proteins involved in genome maintenance, regulating their access to ssDNA and bringing them to their sites of action [2].

*Eco*SSB is one of the most extensively studied ssDNA binding proteins. It consists of four identical subunits (~19 kDa each) that form a functional tetramer [5, 6] (**Figure 1A**) that is stable over a wide range of solution conditions and at sub-nanomolar protein concentrations [4][7]. Each monomer contains an oligonucleotide/oligosaccharide binding (OB) fold that contains the ssDNA binding site [5]. Thermodynamic studies have shown that *Eco*SSB tetramers bind and wrap ssDNA in a variety of binding modes that differ primarily in the number of OB folds that interact with the tetramer [3]. Three different binding modes have been identified on poly(dT) at 25°C, termed $(SSB)_{65}$, $(SSB)_{56}$ and $(SSB)_{35}$, which occlude 65, 56, and 35 nucleotides (nt) per tetramer, respectively, with a fourth mode observed at 37°C that occludes 40 nt [8]. These modes can reversibly interconvert, with the transitions influenced primarily by salt concentration and type as well as protein binding density on the DNA [8]. The $(SSB)_{35}$ mode also binds ssDNA with high cooperativity, forming protein clusters [9-12] that may be important during DNA replication [13]. It has been suggested that SSB utilizes all of these binding modes during its different roles in genome maintenance [13] and that transitions between modes may control access of other proteins to the ssDNA [14, 15].

Crystallographic studies of a C-terminal truncation of the SSB tetramer (SSBc) with two molecules of $(dC)_{35}$ bound suggest a model for the $(SSB)_{65}$ mode in which 65 nt of ssDNA wrap around an SSB tetramer in a topology resembling the seams on a baseball [5] (**Figure 1A**). Based on this structure, a

model for the $(SSB)_{35}$ mode has also been proposed [5]. Less is known about the wrapping configurations of the other binding modes, especially the $(SSB)_{56}$ mode that has only been detected on long poly(dT) ssDNA [8]. However, various techniques such as electron microscopy [16, 17], SSB fluorescence quenching [4, 8, 9, 18, 19] and sedimentation [20] have provided some basic constraints.

Recent single-molecule studies have provided new insights on SSB-ssDNA complex dynamics. Single-molecule FRET (smFRET) measurements characterized transitions between binding modes [21] and established that *Eco*SSB tetramers can diffuse along ssDNA [22] by a reptation mechanism [23]. Force spectroscopy approaches have also proven useful in studying single-stranded DNA binding protein interactions with DNA [24-27]. Force not only adds another variable to perturb protein-DNA interactions but also provides a well-defined reaction coordinate to quantify the energy landscape governing those interactions. Using a combination of optical traps and single-molecule FRET, Zhou *et al*. [23] showed that force gradually unravels ssDNA from *Eco*SSB and proposed that the energy landscape for SSB-ssDNA interactions is smooth, with few barriers to unwrapping.

Here, we present direct observations of a single *Eco*SSB tetramer interacting with ssDNA using force spectroscopy combined with single-molecule fluorescence microscopy. Applying mechanical force to destabilize the SSB-ssDNA complex and facilitate transitions between binding modes, we show that the ssDNA exhibits discrete wrapping states consistent with the known $(SSB)_{65}$, $(SSB)_{56}$ and $(SSB)_{35}$ binding modes. Our results are compatible with putative models of the $(SSB)_{35}$ structure [5] and reveal a likely wrapping configuration for the $(SSB)_{56}$ mode. SSB-$(dT)_{70}$ complexes exhibit reversible force-induced transitions between modes without dissociation and SSB can diffuse along ssDNA in the different binding modes, indicating a highly dynamic complex. The data also reveal details of the energy landscape for SSB-ssDNA interactions. In contrast to previous suggestions [23], the landscape contains multiple barriers between discrete wrapping conformations, suggesting a distinct wrapping pathway for *Eco*SSB. Moreover, the energy density is unbalanced, such that the energy cost of unwrapping increases

as ssDNA is unraveled from its ends. These findings along with studies of the competition between *E. coli* SSB and the RecA recombinase protein demonstrate how SSB bound in its different modes might regulate accessibility to ssDNA of other genome maintenance proteins.

RESULTS

Force Unravels ssDNA from a Single SSB Tetramer

We used dual trap optical tweezers to stretch a SSB-ssDNA complex mechanically. As shown in **Figure 1B**, two trapped functionalized micron-sized beads were tethered together by a DNA construct consisting of a 70-nt poly(dT) ssDNA segment flanked by two long double-stranded DNA (dsDNA) 'handles' (Materials and Methods). The length of the ssDNA was chosen to accommodate one SSB tetramer in its $(SSB)_{65}$ binding mode. We also worked under salt conditions and protein concentrations known to favor the $(SSB)_{65}$ mode in the absence of mechanical tension [8, 21] (Materials and Methods). Force-extension curves (FEC) of this construct in the absence of protein (**Figure 1-figure supplement 1**, green) were in excellent agreement with theoretical models of DNA elasticity (Materials and Methods; **Figure 1-figure supplement. 1**, black dashed line). The total extension of the 'bare' DNA molecule, x_{bare}, is given by the sum of the extensions of the dsDNA handles and the ssDNA binding site at a tension *F*:

$$x_{bare}(F) = \xi_{ds}(F) \cdot N_{ds} + \xi_{ss}(F) \cdot N_{ss} \quad (1)$$

where $\xi_{ds}(F)$ and $\xi_{ss}(F)$ are the extension of one dsDNA base pair and one ssDNA nucleotide given by the extensible worm-like chain [28] and 'snake-like chain' model [29], respectively (Materials and Methods; **Figure 1-figure supplement 2**). N_{ds} = 3,260 bp is the total length of the dsDNA handles and N_{ss} = 70 nt is that of the ssDNA loading site.

To investigate a single SSB tetramer-ssDNA complex, protein in solution was added to the construct (Materials and Methods**; Figure 1B-C**) for a short period of incubation, allowing one SSB to bind the 70-

nt ssDNA. The molecule was then stretched in the absence of free proteins in solution (**Figure 1B-C**). FECs of stretching and relaxing many molecules are shown in **Figure 1D**. The stretching FECs (violet) of the SSB-DNA complex displayed a shorter extension compared to those without protein due to ssDNA compaction by the SSB. Upon stretching to a force >20 pN and relaxing the molecule, the FECs (**Figure 1**, red) matched those in the absence of protein (**Figure 1-figure supplement 1**, green), indicating that the SSB had dissociated during the stretching process. We confirmed that a single SSB was loaded onto the DNA and dissociated at high force through simultaneous fluorescence detection of dye labeled protein. Using an instrument combining optical traps with a single-molecule fluorescence confocal microscope [30], we detected SSB site-specifically labeled with an average of one AlexaFluor555 fluorophore (SSB_f) as we obtained a FEC (**Figure 1-figure supplement 3**; Materials and Methods). The average dissociation force was 10.3 ± 0.9 pN, consistent with previous reports [23]. Integrating the area between protein-bound and bare FECs to the force at which the complex spends half its time bound and half unbound yielded a value for the SSB-ssDNA wrapping free energy of 22 ± 2 k_BT (Materials and Methods) similar to a previously reported value [23].

The difference in extension between stretching and relaxing FECs provides information on the SSB-ssDNA wrapping conformation as a function of force. For SSB-bound DNA, we first considered that SSB adopted the canonical $(SSB)_{65}$ structure [5]. We thus expected a FEC given by Eq. (1) with N_{ss} = 70 – 65 = 5 nt due to occlusion by the SSB. As shown in **Figure 1D**, the stretching FECs (violet) diverged significantly from this theoretical model (black dashed line). **Figure 1E** displays the extension difference, Δx, between the stretching and corresponding relaxing curves as a function of tension F, averaged over many molecules (N = 36; black points), and the corresponding theoretical model (black dashed line). The agreement between model and data at tensions <1 pN is consistent with 65 nt being wrapped around SSB at low forces. Beyond this force, however, Δx is consistently below the prediction, indicating that the SSB wraps <65 nt of ssDNA, in agreement with earlier measurements [23].

Interestingly, neither the data in **Figure 1E** nor in those previous studies [23] provide evidence for discrete wrapping morphologies such as $(SSB)_{56}$ and $(SSB)_{35}$ as observed in ensemble studies. If different SSB modes are stable and interconvertible, discrete transitions in the extension would have been expected in the stretching-relaxing experiment. However, detecting intermediates would be possible only if the rate at which the force was ramped was slower than the transitions between intermediates. Moreover, averaging over multiple molecules here and in Zhou *et al*. [23] likely conceals transitions between SSB-ssDNA wrapping intermediates. Example individual traces (**Figure 1E**, blue, red, and green curves) support this view by illustrating the variability among FECs and their divergence from the average behavior (black). Rips in some of these traces (for example, the red traces at 5 pN) suggest that SSB may undergo transitions between different wrapping states.

SSB Binds ssDNA in Intermediate Wrapping States under Tension

To investigate the presence of intermediate wrapping states further, we measured binding of individual SSB tetramers to the ssDNA at constant tension by operating the optical trap in a force-clamp mode ([31], Material and Methods). As shown in **Figure 2A**, a DNA construct was initially held in the optical tweezers at a desired constant tension (2-10 pN) and protein was added. After a short time, an SSB binds, and the DNA is compacted upon wrapping. At the end of each observation, protein was dissociated by increasing the tension to a force (~25 pN) at which SSB cannot remain stably bound. This cycle was repeated numerous times to monitor new protein binding to the same DNA construct.

Figure 2B shows the change in DNA end-to-end extension, Δx, upon binding of SSB as a function of force. Using bare DNA as a reference (set to 0 nm), negative extension changes correspond to ssDNA wrapping and positive changes to release of wrapped DNA. At low tensions (< 3 pN), we observed that individual SSBs bind and compact ssDNA in a single step (**Figure 2B**). SSBs remained bound to the ssDNA indefinitely at these tensions. In contrast, at higher tensions, (3-8 pN), we observed multiple steps upon

SSB binding, with dynamic transitions among 2 to 3 distinct states (**Figure 2B**, dashed lines) depending on tension, but no dissociation of SSB. We interpret these dynamic changes in extension as wrapping and unwrapping transitions between intermediate conformations of a single ssDNA-SSB complex. Working at low SSB concentrations (0.5 nM) favored the likelihood that multiple SSBs do not bind during one cycle. We corroborated this interpretation with measurements of fluorescently labeled SSB_f. **Figure 2-figure supplement 1** shows that a single SSB tetramer was responsible for the observed wrapping-unwrapping dynamics. Near the dissociation force (9-10 pN), we observed multiple instances of one-step wrapping followed by complete release of ssDNA. At these forces, SSB is unable to bind the DNA tether stably, and the observed transitions correspond to protein binding and dissociation. This interpretation is also confirmed by measurements using fluorescent SSB_f (**Figure 2-figure supplement 1**, right panel), in which dissociation events correlate with loss of fluorescence.

Figure 2C shows the combined extension change distributions from many individual SSBs at different tensions. Similarly to the force-ramp results, Δx decreases as tension increases, indicating that the amount of ssDNA wrapped by SSB decreases. However, in contrast to the force-ramp experiment, the constant force experiment provides evidence for intermediate wrapping conformations of SSB, since multiple states are observed at many tensions. The areas under the peaks in the distributions indicate that SSB spends different amounts of time in these particular states. As tension is increased, the SSB-ssDNA complex shifts to states with smaller Δx, corresponding to lower extents of ssDNA wrapping.

Intermediates Correlate with Different SSB Binding Modes

We considered the possibility that these intermediate DNA wrapping states correspond to the different SSB binding modes observed on poly(dT) in ensemble measurements [8]. **Figure 3A** displays the mean extension changes from the peaks of the distributions in **Figure 2C**. Interpreting these changes in extension, Δx, and attributing these to binding modes required a detailed model. As shown in **Figure**

3B, ssDNA wrapping by SSB contributes in two ways to the extension of the DNA tether: (i) it removes N_w ssDNA nucleotides wrapped by the SSB, and (ii) it adds length due to the effective physical size of the SSB-ssDNA complex, x_{SSB}^{eff}, as noted in other mechanical unfolding studies [32]. The extension of the wrapped DNA molecule, x_{wrap}, is thus:

$$x_{wrap}(F) = \xi_{ds}(F) \cdot N_{ds} + \xi_{ss}(F) \cdot (N_{ss} - N_w) + x_{SSB}^{eff}(N_w, F) \quad (2)$$

The extension change upon wrapping, Δx, is the difference between x_{wrap} and the extension of the bare molecule x_{bare}, given by Eq. (1):

$$\Delta x(F) = \xi_{ss}(F) \cdot N_w - x_{SSB}^{eff}(N_w, F) \quad (3)$$

x_{SSB}^{eff} accounts for the distance between the two ends of the wrapped ssDNA on the SSB (**Figure 3B**). This geometrical term depends on the size of the SSB and the geometry of wrapped ssDNA around the protein, and is thus a function of N_w (and F). For example, based on the proposed model for the $(SSB)_{65}$ structure [5] $x_{SSB}^{eff}(N_w = 65)$ <2 nm since the ends of the wrapped ssDNA exit at nearly the same point on the protein (**Figure 1A**). In the $(SSB)_{35}$ structural model, however, the ssDNA strand exits at opposite ends of the protein and $x_{SSB}^{eff}(N_w = 35)$ is predicted to be ~5.5 nm. x_{SSB}^{eff} must also account for the rotational degree of freedom of the nucleoprotein complex, and only the projection along the direction of the applied force contributes to the extension of the DNA tether. As force F is exerted, a torque is applied on the complex, orienting it along the direction of tension. This effect is modeled by

$$x_{SSB}^{eff}(N_w, F) = x_{SSB}(N_w) \cdot L(F x_{SSB} / k_B T) \quad (4)$$

where x_{SSB} is the distance between wrapped ssDNA ends in the protein's frame of reference (**Figure 3B**) and $L(z) \equiv \coth(z) - 1/z$ is the orientation factor, derived from the alignment of a particle undergoing rotational Brownian motion to an external torque (Materials and Methods).

Substituting Eq. (4) into (3) provides an expression for the measured extension change Δx at each force F in terms of the SSB-ssDNA configuration parameters N_w and x_{SSB}. Thus, for each data point

$\Delta x(F)$ in **Figure 3A** there exists a set of possible values for the pair N_w and x_{SSB} (Materials and Methods). **Figure 3-figure supplement 1** displays how selected data points from **Figure 3A** each project onto a curve of allowed values in the space of N_w and x_{SSB} (colored lines). Structural considerations limit the range of possible N_w and x_{SSB}. The fact that x_{SSB}^{eff} can be no greater than the size of the SSB (i.e. $0 < x_{SSB} < 6.5$ nm) places a restriction on the range of possible values N_w can have for each Δx (**Figure 3-figure supplement 1** left panel, dotted colored lines; **Figure 3C** dotted colored lines). We limited the range of N_w further by utilizing the $(SSB)_{65}$ structure [5] to restrict the potential geometries of any intermediate wrapping states. By measuring the end-to-end distance between every pair of nucleotides separated by N_w nt along the ssDNA in the structural model, we imposed a lower and upper bound on x_{SSB} at each force F (**Figure 3-figure supplement 1** middle panel, gray contours and shaded area; Materials and Methods). This refined range of possible N_w restricts our observed wrapping intermediates to four bands centered around N_w = ~65, 50-60, 30-40, and 10-20 nt (**Figure 3C** dashed colored lines). The first three correspond well with the $(SSB)_{65}$, $(SSB)_{56}$, and $(SSB)_{35}$ wrapping states observed at 25°C on poly(dT).

A better estimate for x_{SSB} and N_w at each force F was obtained by recognizing that specific amino acid residues within *Eco*SSB are known to contact the ssDNA. Trp-40, Trp-54, Trp-88 and Phe-60 have been shown to play important roles in maintaining protein-DNA stability [33-35]. Crystal structure analysis also implicates Trp-54 and Arg-56 as important in creating pockets of positive electrostatic potential on the SSB surface for ssDNA to bind [5]. Lastly, a DNA density map generated by all-atom molecular dynamics simulations of SSB [36] in solution with free oligonucleotides showed that DNA interacts most strongly to regions on each monomer near residues 54-56 (Trp-88 and Phe-60 are also located near this region) (**Figure 3-figure supplement 1** right schematic, residues highlighted in green; Materials and Methods). Based on these results, we identified the Trp-54/His-55/Arg-56 cluster as a 'hotspot', residues on each SSB monomer that may serve as anchor points along the DNA wrapping path

on the SSB. Our best estimates for N_w at each force F, shown in **Figure 3C** (colored points), were obtained by considering the distances between groups of nucleotides near each hotspot (**Figure 3-figure supplement. 1** right panel, black contours; Materials and Methods).

Our models consistently show that ssDNA unwraps in discrete steps with tension, instead of gradually as proposed previously [23]. As tension increases from 0-8 pN, the number of wrapped nucleotides decreases in a stepwise manner from 65 to 56 to ~35 nt (**Figure 3C**, purple, blue, and green points, respectively), matching very well to the known binding modes. The best estimates for N_w and x_{SSB} also generate models for the ssDNA wrapping conformations for each intermediate (**Figure 3C**; schematics and **Figure 3-fiugre supplement 2**). Control experiments using an SSB mutant confirm our analysis. Mutation of Trp-54 to Ser was previously shown to disrupt interactions with ssDNA and favor wrapping in the $(SSB)_{35}$ mode [35]. We similarly found that the number of nucleotides wrapped by this mutant was lower than that of the wild type SSB, with N_w = 35 nt being the most probable wrapping conformation over the range of tensions assayed (**Figure 3-figure supplement 3**).

SSB in Intermediate Wrapping States Can Diffuse on ssDNA

We next investigated whether the different wrapping states of SSB affect its dynamics on ssDNA, in particular its ability to diffuse. We monitored simultaneously the wrapping state of SSB and its position on ssDNA using the combined optical tweezers-confocal fluorescence microscope. We measured the latter using smFRET between the DNA construct modified with a single acceptor fluorophore (Cy5) at the 5' ss-dsDNA junction and fluorescent SSB_f labeled with an average of one donor fluorophore (AlexaFluor555) (**Figure 4A**).

Upon SSB_f binding to ssDNA held at a constant 5 pN tension, we observed transitions between the two wrapping states with N_w = 35 nt and 56 nt, based on the analysis from the previous section. We also observed transitions between two FRET states with high (E ~ 0.5) and low FRET efficiencies (E ~ 0)

corresponding to SSB_f positioned at the 5' ss-dsDNA junction vs. the 3' end, respectively. As shown in **Figure 4B**, all four combined extension-FRET states could be detected in our data: 'i' – 35 nt wrapping and low FRET, 'ii' – 35 nt wrapping and high FRET, 'iii' – 56 nt wrapping and high FRET, and 'iv' – 56 nt wrapping and low FRET. Inspection of individual time traces revealed cases in which transitions in extension and FRET were correlated. **Figure 4C** (left) shows an example of such a transition from state i -> iii -> i, in which an SSB in $(SSB)_{35}$ mode wraps an additional ~20 nt of ssDNA from the 5' end into $(SSB)_{56}$ mode, then releases the same end of DNA. This confirms our interpretation that these changes in extension represent transitions between binding modes. Alternately (**Figure 4C**; middle and right) we observed cases in which FRET transitions occurred independently of changes in wrapping state. The two-state time traces indicate SSB diffusing across the sensitive distance range of smFRET (about one Förster radius, ~6 nm = 18 nt [37]) and support a reptation mechanism for SSB diffusion (**Figure 4-figure supplement 1**), as previously proposed [23]. Diffusion of SSB occurred in both $(SSB)_{35}$ (**Figure 4C**; middle) and $(SSB)_{56}$ (**Figure 4C**; right) wrapping modes. We reasoned that the lifetimes of the high FRET states in these traces correspond approximately to the time the protein takes to diffuse by one Förster radius from the ss-dsDNA junction, and estimated a diffusion constant $D \approx 27$ nt^2/s for the $(SSB)_{35}$ mode and 15 nt^2/s for the $(SSB)_{56}$ mode. This range of values is consistent with prior reports [22] when accounting for temperature (~23°C in our measurements) and the expected reduction in D due to the 5 pN tension [22, 23]. We observed no examples (0 of $N = 82$) of transitions from state i -> iii -> ii—wrapping one end of DNA and releasing the other—providing no support for a 'rolling' mechanism of diffusion [38] (**Figure 4-figure supplement 1**).

Discussion

Due to its homotetrameric nature, the *Eco*SSB protein can bind ssDNA in a number of different modes that differ in the number of nucleotides occluded in complexes with long ssDNA [3, 8, 21]. SSB-

ssDNA complexes can transition between these modes *in vitro* and their stabilities can be modulated by changes in solution conditions (salt, pH, temperature) as well as the SSB to DNA ratio. Our experiments show that force can also be used to control the ssDNA wrapping state of *Eco*SSB. This has revealed stable intermediate states of $(dT)_{70}$ ssDNA wrapping around a single SSB tetramer that correlate well with the known [NaCl]-induced poly(dT) binding modes, $(SSB)_{65}$, $(SSB)_{56}$, $(SSB)_{35}$ that have been observed for SSB binding to longer poly(dT) [4, 8].

The observation of stable force-induced SSB-$(dT)_{70}$ intermediates provides new details about the likely wrapping topologies of the different binding modes. Our results are consistent with the ssDNA wrapping topology proposed for the $(SSB)_{65}$ mode based on a crystal structure (**Figure 3C**; schematic, and **Figure 3-figure supplement 2**) [5]. They also suggest that the $(SSB)_{56}$ mode has ssDNA bound to all four subunits, but with the 3' terminal ssDNA end unraveled to the nearest hotspot (**Figure 3C**; schematic, and **Figure 3-figure supplement 2**). This model is consistent with studies [18, 19] suggesting that all 4 monomers of an SSB tetramer interact with ssDNA upon binding a molecule of $(dT)_{56}$. At forces in the range of 5-8 pN, we observe between 1 to 3 separate states wrapping 30-40 nt. Our data and analysis are not sensitive enough to ascribe specific wrapping conformations to each. We believe at least two conformations wrapping ~35 nt are consistent with the observed extension changes, one of which is nearly identical to the proposed $(SSB)_{35}$ structure [5] (**Figure 3C** schematic, and **Figure 3-figure supplement 2**). Interestingly, prior studies [21] have suggested the existence of an alternate "$(SSB)_{35b}$" mode that occludes 35 nt but is structurally distinct from $(SSB)_{35}$, consistent with our observations. At tensions >8 pN, we also observed a stable intermediate reflecting ~17 nt of bound ssDNA [18, 19, 39]. Here, a multitude of wrapping conformations around two monomers is consistent with the data (**Figure 3C** schematic, and **Figure 3-figure supplement 2**). Although fluorescence quenching studies [39] suggest that $(dT)_{16}$ would bind to one monomer of SSB, partial interactions with two monomers in our structural model may sum to those of a monomer. It is possible that near dissociation, wrapping geometries could

be more heterogeneous. Prior studies have shown that *Eco*SSB can bind to ssDNA as short as $(dT)_8$ [40]. However, we do not observe long-lived intermediates wrapping less than ~17 nt before SSB dissociation.

Analyzing the transitions between wrapping intermediates (**Figure 2B**) reveals that almost every transition (*N* = 373 out of 380 total, 98%) occurs between adjacent wrapping states, i.e. between $(SSB)_{56}$ and $(SSB)_{35}$, but never directly between $(SSB)_{56}$ and $(SSB)_{17}$. This suggests a single, linear kinetic pathway for wrapping (**Figure 3-figure supplement. 2**, right to left) and unwrapping (left to right). This proposed pathway is corroborated by measurements of *E. coli* SSB in competition with RecA for ssDNA. As shown in **Figure 5A-B**, we first loaded a single SSB tetramer onto ssDNA at a force of 5 pN, where our analysis shows the protein interconverts between the $(SSB)_{56}$ and $(SSB)_{35}$ modes. We then added RecA to the complex under conditions favoring polymerization into ssDNA-RecA filaments (Materials and Methods). [To prevent polymerization of RecA onto the dsDNA handles, the construct was synthesized with the 70-nt ssDNA loading site flanked by short non-DNA spacers (Materials and Methods)]. In the absence of SSB, RecA extends the construct by ~10 nm as it fills the ssDNA (**Figure 5-figure supplement 1**), consistent with previous reports that ssDNA-RecA filaments are 50% longer than dsDNA [41, 42] (Materials and Methods). When RecA is added to ssDNA wrapped by a single SSB, RecA takes longer to polymerize but eventually removes the SSB in a stepwise fashion (**Figure 5C**). Analyzing the measured extension changes from many measurements (**Figure 5D**; Materials and Methods) reveals that the SSB is unraveled in discrete steps, corresponding to the same pathway of intermediates, $(SSB)_{35}$ -> $(SSB)_{17}$ -> unbound, as proposed above (**Figure 3-figure supplement 2**).

The ability to measure the extension of each wrapping state as a function of force also allows us to construct an energy landscape for the SSB-ssDNA complex. Using the extension histograms in **Figure 2C**, we determined the probabilities of occupying specific wrapping modes at each force, and from these we calculated the free energy differences between modes (Materials and Methods; for simplicity, we ascribed intermediates with similar N_w to the same wrapping state). We also used the lifetimes of each

wrapping state and transition probabilities at each force (**Figure 2B**) to estimate the barrier heights between states (Materials and Methods). Our analysis (**Figure 6**) shows that the free energy of wrapping into the $(SSB)_{65}$ mode is 21 ± 1 k_BT, in excellent agreement with the area between protein-bound and bare FECs (22 ± 2 k_BT; **Figure 1D**). Interestingly, this wrapping free energy is not distributed evenly among the 65 nt. Instead, we find that 73% of the energy is concentrated in the first 35 nt wrapped (energy density = 0.44 ± 0.02 k_BT/nt). In contrast, the $(SSB)_{65}$ and $(SSB)_{56}$ states are separated by only ~0.7 k_BT (energy density ~0.07 k_BT/nt). This finding suggests that the last ~10 nt wrapped are more susceptible to unraveling and thus might be more accessible to other proteins competing for ssDNA. This unbalanced energy density profile may provide a mechanism by which SSB is displaced by the recombinase RecA, which requires a foothold of 6-17 nt to polymerize into filaments [43, 44]. We note that in the RecA/SSB competition experiment (**Figure 5**), we observe RecA filaments forming only once the SSB transitions to the $(SSB)_{35}$ mode, granting access to >14 nt of ssDNA.

Our measurements that SSB can diffuse on ssDNA while in different wrapping modes provide insights into how SSBs could be redistributed along ssDNA by other proteins seeking access to ssDNA. The observation of SSB-ssDNA rearrangements without unwrapping or rewrapping (**Figure 4**) points to a sliding mechanism of diffusion in which ssDNA reptates along the protein, consistent with prior models [23]. In **Figure 5**, we believe RecA polymerization likely slides the SSB to one ssDNA-dsDNA junction prior to unravelling it [22, 43]. Interestingly, the data in **Figure 4** suggest that diffusion may be faster in the $(SSB)_{35}$ mode. The transition rates between FRET states are ~1.8X larger in the $(SSB)_{35}$ mode than in the $(SSB)_{56}$ mode. The observation that a smaller site size leads to faster diffusion is consistent with reports that human RPA, which covers 30 nt, has a larger diffusion coefficient than *Eco*SSB in its $(SSB)_{65}$ mode [45].

Previous work has proposed that different wrapping modes may be used selectively in different DNA metabolic processes (e.g. replication vs. recombination) [13, 46]. How and which of these modes

are used for particular processes remains unclear, as experimental proof of this proposition has proven difficult to obtain *in vitro*. We anticipate that the control of SSB wrapping mode by applied force may be a useful experimental tool to test this hypothesis.

MATERIALS AND METHODS

Sample preparation

SSB, fluorescently labeled SSB, and RecA

Both wild-type and fluorescently labeled *E. coli* SSB were expressed and purified as described previously [22, 47], with an addition of a double-stranded DNA cellulose column to remove a minor exonuclease contaminant [7]. The labeled SSB was single-point mutated from Ala to Cys at position 122 in the C-terminus, and labeled with AlexaFluor555 maleimide (Invitrogen, Grand Island, NY) to the extent of ~25% (~1 dye per tetramer) as described previously [22]. *E. coli* RecA was purchased from New England Biolabs (M0249S; Ipswich, MA).

Single-stranded DNA Construct

The single-stranded DNA construct consisted of three separate fragments ligated together (**Figure 1-figure supplement 5**): 'Right Handle' (RH), 'Left Handle' (LH), and 'Binding Site' (BS). The handles served as functionalized linkers that connected to trapped beads through biotin-streptavidin and digoxigenin-anti-digoxigenin linkages and spatially separated the beads from the protein binding site. LH was synthesized from PCR amplification of the PBR322 plasmid (New England Biolabs, Ipswich, MA) using a 5'-biotin-labeled primer and digested to a 1550-bp length with the PspGI restriction enzyme (New England Biolabs, Ipswich, MA), leaving a 5-nt 5' overhang. RH was PCR-amplified from the phage lambda DNA (New England Biolabs, Ipswich, MA) using a 5'-digoxigenin-labeled primer and digested with the TspRI restriction enzyme (New England Biolabs, Ipswich, MA), resulting in a 1710-bp dsDNA with a 9-nt 3' overhang.

The last fragment of the construct, BS, consisted of a 70-nt poly(dT) oligodeoxyribonucleotide flanked by sequences complementary to both overhangs of LH and RH: 5'-CCTGG $(T)_{70}$ CCCACTGGC-3'. In some experiments, a Cy5 fluorescence dye was attached directly to the DNA backbone using

phosphoramidite chemistry at the location between the 5' complementary sequence and the 70-nt poly(dT) region. The final construct had one digoxigenin and one biotin on opposing ends for linkages to anti-digoxigenin- and streptavidin-coated beads, respectively. All oligonucleotides were custom-ordered from Integrated DNA Technologies (Coralville, IA).

In the experiments with RecA, BS was modified to contain two internal 18-atom hexa-ethylene-glycol spacers (iSp18; Integrated DNA Technology, Coralville, IA) between the 70-nt poly(dT) and the complementary overhangs. This modification prevented RecA filament formation onto the dsDNA handles (**Figure 5A**, cyan). The BS fragment was ligated to RH and LH to form a complete construct.

Instrument Design

Optical Tweezers

Experiments were performed using a high-resolution dual optical trap instrument combined with a confocal microscope as previously described [30]. The dual traps were formed by timesharing a single IR laser (a 5-W, 1064-nm diode-pumped solid-state laser, YLR-5-1064-LP; IPG Photonics, Oxford, MA), by intermittently deflecting the laser between two angles with an acousto-optic modulator (AOM; IntraAction Corp., Bellwood, IL). The instrument was housed in a temperature-controlled room at ~23°C.

The IR beams were tightly focused by a 60x, water-immersion microscope objective (Nikon, Tokyo, Japan) to form two optical traps inside the sample chamber. Each trap held a single polystyrene bead during an experiment. Bead displacements were detected by back-focal plane interferometry: forward-scattered laser light was collected by a second identical objective lens, imaged onto a quadrant photodiode detector (QPD), and analyzed. In all experiments, both traps were calibrated by measuring the power spectral density of bead Brownian motion. Trap stiffnesses were typically equal to 0.3 pN/nm.

Fluorescence probes were excited by a 532-nm 5-mW laser (DPGL-05S, World Star Tech, Toronto, ON, Canada) interlaced with the trapping IR laser at a rate of 66 kHz [30]. Fluorescence light from donor and acceptor dyes emitted from within a confocal volume was collected by the front objective, band-pass filtered, focused through a 20-µm pinhole, and imaged onto two avalanche photodiodes (APD) (PerkinElmer, Waltham, MA). The AlexaFluor555 emission passed through a 580-nm low-pass filter (Chroma Technology Corp., Bellows Falls, VT) to one APD, and the Cy5 emission through a 680-nm low-pass filter to the second APD.

Flow Chamber

A custom-designed laminar flow chamber ([48], **Figure 1 figure supplement 4**), consisting of two glass coverslips (12-545-M, 24 x 60-1, ThermoFisher, Waltham, Massachusetts) sandwiching melted Nescofilm (Karlan, Phoenix, AZ) was patterned with channels. Eight holes with a diameter of 2 mm were drilled onto one of the coverslips by a laser engraver system (VLS2.30; Universal Laser Systems, Scottsdale, AZ) to create four inlets and four outlets. The Nescofilm was cut into three separate channels using the same laser system. Top and bottom channels were connected to a central channel through glass capillaries (OD = 100 ± 10 µm, ID = 25.0 ± 6.4 µm; Garner Glass Co., Claremont, CA). The chamber was mounted onto an anodized aluminum frame into which inlet and outlet tubing (ABW00001; Tygon, Saint-Gobain, Akron, OH and PE20; Intramedic, Becton Dickinson and Company, Sparks, MD) was connected.

Three syringe pumps (PHD 2000 Infusion; Harvard Apparatus, Holliston, MA) were used to control the flow through the different channels: top, central, and bottom, separately (**Figure 1-figure supplement 4**). The top and bottom channels were injected with anti-digoxigenin and streptavidin beads, respectively. In the central channel, two streams of appropriate buffers were pumped at a speed of 140 µm/s (~100 µL/hr) and merged to form a laminar interface. In a typical experiment, a DNA

molecule tethered between trapped beads could be moved across the interface using a motorized stage controller in ~2 s.

Optical Tweezers Experiment

Except where otherwise noted, experiments were performed in a working buffer containing 100 mM Tris-HCl (pH 7.6), 10 mM NaCl, 0.1 mM EDTA. An oxygen scavenging system (pyranose oxidase (P4234; Sigma-Aldrich, St. Louis, MO) and catalase (219001; EMD Millipore, Billerica, MA)) was added to increase tether and fluorescence photobleaching lifetime [49]; to this buffer, 0.5 nM of SSB protein was added. For the measurements involving fluorescence, an oxygen triplet-state quencher (Trolox; Sigma-Aldrich, St. Louis, MO) was added to the working buffer to prevent fluorophore blinking [50]. Experimental conditions were chosen to be compatible with the optical trapping assay and to favor the $(SSB)_{65}$ mode in the absence of force. The $(SSB)_{65}$ mode is known to be stabilized at high [NaCl] (>200 mM), the $(SSB)_{56}$ mode at intermediate [NaCl] (50-100 mM), and the $(SSB)_{35}$ mode at low [NaCl] (10 mM) [8]. Mg^{2+} and polyamines also facilitate formation of the high site size modes [8, 51]. We independently verified that the $(SSB)_{65}$ mode was favored in the experimental conditions above (100 mM Tris-HCl, low SSB concentration), by measuring a binding isotherm using fluorescence of Cy5-$(dT)_{70}$-Cy3-dT with SSB (**Figure 1-figure supplement 6**).

In all experiments, a single-stranded DNA construct was first tethered between a trapped streptavidin-coated bead and an anti-digoxigenin-coated bead in buffer. The tether was then stretched under tension to obtain a force-extension curve (FEC). The FEC was used to check behavior of the tether by verifying it against a theoretical polymer model (**Figure 1-figure supplement 1**).

Force-ramp experiment: A tether was moved into the SSB stream at low tension to allow a single SSB to bind (**Figure 1-figure supplement 4**, Position 2). After a period of incubation, the tether was moved back to the blank buffer (Position 1) to ensure that no other SSBs were present during experiment. To

observe single SSB unwrapping, a force-ramp experiment was performed by increasing the trap separation at a rate of ~65 nm/sec until the tether tension reached ~25 pN. The tether was then relaxed back at the same rate to the original starting position.

Constant force experiment: Constant force experiments were performed with a PID controller loop that monitored the trapped bead positions and controlled the trap separation to maintain a constant tension on a tethered DNA molecule. The constant force experiment was initiated in the blank buffer stream at constant tensions ranging from 2 to 11 pN (**Figure 1-figure supplement 4**, Position 1). While keeping tension constant, the tether was moved into the SSB stream to allow a single SSB to bind (Position 2). After an SSB bound, the tether was moved back to the blank buffer stream for observation.

RecA-SSB competition experiment: These experiments were performed in a working buffer containing 20 mM Tris(OAc), pH 7.5, 10 mM NaCl, 4 mM $Mg(OAc)_2$, and an oxygen scavenging system. The experiment was initiated in a buffer stream containing 0.5 nM of SSB only at a constant tension of 5 pN (**Figure 5A-B**). After an SSB bound (**Figure 5B**; Position 1), the tethered construct was moved into the buffer stream containing 125 nM of RecA and 125 μM ATP-γS for observation (Position 2). ATP-γS (A1388; Sigma-Aldrich, St. Louis, MO) was included to stabilize the RecA filament.

Data Analysis

Single-stranded DNA Polymer Modeling

The total extension of the tether was decomposed into dsDNA and ssDNA components as shown in Eq. (1). The extension of each of these segments was computed separately. The dsDNA segment was modeled with an extensible worm-like chain (XWLC) [28]. Parameters for dsDNA were obtained from the literature [52]; we used a persistence length of 53 nm, a stretch modulus of 1,200 pN, and a contour length per base pair of 0.338 nm bp^{-1}. The ssDNA segment was fitted to the recently reported "snake-

like" chain model [29]. Parameters were obtained by comparing the amount of salt (monovalent ion) used in our buffer to the lookup table provided [29]. Representative FECs of the DNA construct containing 3,260 bp dsDNA and 70 or 140-nt poly(dT) ssDNA (**Figure 1-figure supplement 2**; green and orange, respectively) were fitted to the model (black dashed and dotted lines, respectively). FEC data of both constructs were in excellent agreement with theoretical models of DNA elasticity.

We validated the use of the snake-like chain model for ssDNA of varying lengths by subtracting FECs of a construct containing a 70-nt ssDNA site (red) from those of a construct with a 140-nt poly(dT) ssDNA site (orange) at each force. The resulting extension difference (**Figure 1-figure supplement 2**, inset) displayed an excellent agreement with the snake-like chain model for 70 nt (black dashed line). (The extension difference was also used to determine one of the parameters of the snake-like chain model, the ssDNA extension at 20 pN [29]. For 70-nt ssDNA, this was determined to be ~35 nm.)

SSB-ssDNA Complex Modeling

Modeling the effect of SSB-ssDNA complex size on extension: Equation (2) models the extension of SSB-wrapped DNA. The second term in the expression represents the extension due to the remaining $N_{ss} - N_w$ nucleotides of ssDNA unwrapped by the protein, and the third represents the contribution to the extension from the physical size of the SSB-ssDNA complex. For the latter, we approximated the ssDNA-wrapped SSB as a rigid body of size x_{SSB} that is able to diffuse rotationally. The effect of tension F on the ssDNA is to orient the complex along the direction of tension. The energy associated with orienting the SSB-ssDNA complex is given by:

$$E_{orient} = -\vec{F} \cdot \vec{x}_{SSB} = -F x_{SSB} \cos\theta \,,$$

where $\vec{F}$ is the force vector, $\vec{x}_{SSB}$ the vector defined by the entry and exit points of the wrapped ssDNA on the protein (**Figure 3B**), and θ is the angle between the two vectors. The effective size of the SSB, i.e.

that which contributes to the measured extension, is given by the projection of $\vec{x}_{SSB}$ onto the force axis, $x_{SSB}^{eff} = x_{SSB}\langle\cos\theta\rangle$, where $\langle\cdots\rangle$ denotes the thermal average. This average is obtained by integrating a Boltzmann distribution of orientation energies over all possible orientation angles θ, φ:

$$\langle\cos\theta\rangle = \frac{\int_0^{2\pi} d\varphi \int_0^{\pi} \sin\theta d\theta \cos\theta \exp(-Fx_{SSB}\cos\theta/k_BT)}{\int_0^{2\pi} d\varphi \int_0^{\pi} \sin\theta d\theta \exp(-Fx_{SSB}\cos\theta/k_BT)}.$$

Note that θ, φ correspond to the angles in a spherical coordinate system with force pointing along the *z*-axis. Carrying out the integrals yields:

$$\langle\cos\theta\rangle = \coth\left(\frac{Fx_{SSB}}{k_BT}\right) - \frac{k_BT}{Fx_{SSB}},$$

known as the Langevin function, $L(Fx_{SSB}/k_BT)$ in Eq. (4), first derived for the classical model of paramagnetism [53]. The same expression has also been used to model protein size effects in mechanical unfolding studies [54]. For forces $F >> k_BT/x_{SSB}$, the complex aligns with the force vector and $\langle\cos\theta\rangle \approx 1$.

Determination of SSB wrapping conformation from extension change data: Equations (3) and (4) relate the measured extension change Δx at each force F to the number of wrapped nucleotides, N_w, and the distance between ssDNA entry and exit points on the SSB, x_{SSB}. Substituting Eq. (4) into (3) and solving for N_w yields

$$N_w = \frac{\Delta x(F) + x_{SSB}\coth(Fx_{SSB}/k_BT) - k_BT/F}{\xi_{ss}(F)} \quad (5)$$

where the definition of the Langevin function $L(z)$ was used. Entering an extension change data point $\Delta x(F)$ and ssDNA elasticity model value $\xi_{ss}(F)$ into Eq. (5) at a given force F yields a single-valued function of N_w in terms of x_{SSB}. The functions $N_w(x_{SSB})$ represent the set of allowable values of the pair

500 x_{SSB}, N_w for each extension change data point $\Delta x(F)$, and are plotted as colored curves in **Figure 3-figure**
501 **supplement 1** for selected data points from **Figure 3A**. The widths of the curves correspond to the error
502 bars in **Figure 3A**.

503 We restricted the range of allowable values for N_w by placing upper and lower limits on x_{SSB}, $x_{SSB,max}$
504 and $x_{SSB,min}$, based on structural constraints. At coarsest level, x_{SSB} is bounded by the size of the protein,
505 such that $x_{SSB,min} = 0$ and $x_{SSB,max} = 6.5$ nm. This provided upper and lower limits on N_w for each data point
506 $\Delta x(F)$ (**Figure 3-figure supplement 1** left panel, dotted colored lines). A stricter set of constraints was
507 obtained from the maximum and minimum end-to-end distances between pairs of wrapped nucleotides
508 n_i and n_j separated by N_w nt (i.e. $|n_i - n_j| = N_w - 1$). We used the SSB-ssDNA crystal structure [5] to
509 determine these bounds, $x_{SSB,max}(N_w)$ and $x_{SSB,min}(N_w)$ (**Figure 3-figure supplement 1** middle panel, gray
510 contours and shaded area). The intersection points between the curves generated by Eq. (5) and
511 $x_{SSB,max}(N_w)$ and $x_{SSB,min}(N_w)$ provided a tighter set of limits on N_w for each data point $\Delta x(F)$ (**Figure 3-**
512 **figure supplement 1** middle panel, dashed colored lines).

513 The best estimates for N_w were obtained by considering 'hotspots' of interactions. Clusters of
514 residues on the SSB tetramer to which nucleotides preferentially associated were determined from the
515 SSB crystal structure [5], biochemical studies [5, 34, 35], and recent all-atom molecular dynamics (MD)
516 simulations [36]. In the latter, a density map of DNA on *Eco*SSB was generated from MD simulations of
517 the protein with free nucleotides in solution. The density map was extracted from the atomic trajectory
518 by replacing each C1' atom on the nucleotide with a Gaussian distribution with standard deviation equal
519 to the van der Waals radius of the atom. This process was repeated at every frame of the simulation
520 trajectory and the result temporally averaged. The resulting density map was then spatially averaged
521 with maps produced by rotation about each symmetry axis of the homotetramer (Maffeo, personal
522 communication). The regions of highest DNA density were found to be located near the Trp-54, His-55,

and Arg-56 residues, consistent with their known role in maintaining protein-DNA stability [5, 34, 35] (**Figure 3-figure supplement 1**, green molecular surfaces).

Nucleotides in the wrapped ssDNA interacting with these 'hotspots' were determined based on the distance between their phosphate groups and the amino acid residues 54-56. Utilizing the SSB crystal structure, 6-7 nt per hotspot were found within a 5-7 Å distance. The set of distances, x_{SSB}, and number of nucleotides, N_w, between groups of nucleotides associated with each hotspot were then calculated and a smooth contour spanning the range of that set determined (**Figure 3-figure supplement 1** right panel, black numbered contours). The intersection points between the curves generated by Eq. (5) and the contours from the above hotspot analysis provided the tightest set of limits on N_w for each data point $\Delta x(F)$ (**Figure 3-figure supplement 1** right panel, shaded colored areas). We selected the center of the range as the best estimate for N_w (black dots). These served as a basis for determining the possible wrapping conformations of the complex (**Figure 3C** colored points).

RecA-SSB competition model

The extension of ssDNA is known to increase by 50% compared to B-form dsDNA upon binding by RecA [41, 42]. Thus, the extension of the construct fully polymerized with RecA, x_{RecA}, is given by:

$$x_{RecA}(F) = \xi_{ds}(F) \cdot N_{ds} + 1.5\xi_{ds}(F) \cdot N_{ss} \quad (6)$$

where N_{ds} = 3,260 bp is the total length of the dsDNA handles and N_{ss} = 70 nt is that of the ssDNA loading site. Subtracting Eq. (6) from the extension of the bare DNA molecule, x_{bare}, given by Eq. (1), gives the extension change:

$$\Delta x(F) = 1.5\xi_{ds}(F) \cdot N_{ss} - \xi_{ss}(F) \cdot N_{ss}$$

which is ~10 nm at F = 5 pN, closely matching observations (**Figure 5-figure supplement 1**).

In measurements of RecA displacing a bound SSB (**Figure 5**), the extension change includes contributions from SSB alone, RecA with SSB, and RecA alone on ssDNA. The first and last of these are

given by Eqs. (2) and (6), respectively. A molecule loaded with N_w nucleotides wrapped by an SSB, and the remaining $N_{ss} - N_w$ nucleotides loaded with RecA, on the other hand, has an extension:

$$x_{SSB+RecA}(F) = \xi_{ds}(F) \cdot N_{ds} + 1.5\xi_{ds}(F) \cdot (N_{ss} - N_w) + x_{SSB}^{eff}(N_w, F) \quad (7)$$

In **Figure 5D**, five distinct states are observed. These are well modeled by the following: (i) one SSB in the $(SSB)_{56}$ binding mode with no RecA bound [Eq. (2) with N_w = 56 nt], (ii) one SSB in the $(SSB)_{35}$ binding mode with no RecA bound [Eq. (2) with N_w = 35 nt], (iii) one SSB in the $(SSB)_{35}$ binding mode with all remaining unwrapped nucleotides fully loaded with RecA [Eq. (7) with N_w = 35 nt], (iv) one SSB in the $(SSB)_{17}$ binding mode with all remaining unwrapped nucleotides fully loaded with RecA [Eq. (7) with N_w = 17 nt], (v) no SSB bound, RecA fully polymerized on the ssDNA [Eq. (6)].

Energy Landscape

Determination of wrapping intermediate energies: The energy landscape of the SSB-ssDNA nucleoprotein complex was estimated from FECs and from data of wrapping conformation vs. force. First, the total free energy of wrapping, G_{wrap}, was estimated from the area between FECs of the protein-bound and bare DNA molecules, $x_{wrap}(F)$ and $x_{bare}(F)$ (see Eq. (1) and (2) and **Figure 1**), integrated to the average SSB dissociation force. The free energy of the protein-bound DNA molecule to a force F is given by:

$$G_{SSB-bound}(F) = G_{wrap} + \int_0^F x_{wrap}(F')dF'$$

whereas that of the bare, protein-free DNA is $G_{bare}(F) = \int_0^F x_{bare}(F')dF'$. Both integrals represent the free energy of stretching to force F. At the dissociation force $F_{1/2}$, the probabilities that an SSB is wrapped or unwrapped are equal, i.e. the two free energies are equal. It follows that:

$$G_{wrap} = \int_0^{F_{1/2}} (x_{bare}(F') - x_{wrap}(F'))dF'$$

569 which is the negative area between the FECs in **Figure 1**.

570 The remaining features of the energy landscape were determined from the wrapping conformation
571 probabilities vs. force. The presence of four wrapping conformations, $(SSB)_{65}$, $(SSB)_{56}$, $(SSB)_{35}$, $(SSB)_{17}$,
572 and an unwrapped state implies that the energy landscape is dominated by five potential wells.
573 Applying force to the complex tilts the energy landscape [55], and changes the free-energy difference
574 between these states. The probability the complex adopts a particular wrapping state *i* at force *F* is
575 given by the Boltzmann distribution, i.e.

576 $$p_i(F) \propto e^{-(G_i + G_{stretch}(F))/k_B T} \tag{8}$$

577 where G_i is the free energy of state *i* and $G_{stretch}(F) = \int_0^F x_i(F')dF'$ is the free energy of stretching the SSB-
578 ssDNA complex in state *i* to force *F*. The free energy difference between two states *i* and *j* can,
579 therefore, be expressed as

580 $$\frac{p_i(F)}{p_j(F)} = e^{-(\Delta G_{ij} + \Delta G_{stretch}(F))/k_B T} \tag{9}$$

581 where $\Delta G_{ij} = G_i - G_j$ and $\Delta G_{stretch}(F) = \int_0^F (x_i(F') - x_j(F'))dF'$.

582 As described in the text, each peak in the histograms of extension change vs. force in **Figure 2** was
583 assigned a particular wrapping state *i*, as detailed in **Figure 3**. We determined the probability $p_i(F)$ from
584 the ratio of the area under the peak to the total area in the histogram at force *F*, (**Figure 6-figure**
585 **supplement 1**). From Eq. (9), we determined the free energy difference between pairs of states,
586 evaluating $\Delta G_{stretch}(F)$ from the area between curves of extension vs. force for the two wrapping states *i*
587 and *j* according to Eq. (2). Since some of the same states were populated at different forces, we
588 obtained several estimates of the same free energy differences. All yielded consistent values, which
589 were averaged together and used to calculate a standard error. Setting the free energy of the

unwrapped state $G_0 = 0$, the free energy associated with each state was calculated to be $G_{17} = -6.80 \pm 0.82\ k_BT$, $G_{35} = -15.38 \pm 0.57\ k_BT$, $G_{56} = -20.39 \pm 0.83\ k_BT$, and $G_{65} = -21.11 \pm 0.83\ k_BT$. The corresponding energy landscape is presented in **Figure 6**.

Determination of barrier heights: The barrier heights for the energy landscape of the SSB-ssDNA nucleoprotein complex were estimated from lifetime measurements of the different wrapping conformations vs. force as shown in **Figure 2**. The four identified wrapping conformations, $(SSB)_{65}$, $(SSB)_{56}$, $(SSB)_{35}$, $(SSB)_{17}$, and the unwrapped state undergo force-induced transitions between each other according to the following linear kinetic pathway:

$$0 \rightleftharpoons 17 \rightleftharpoons 35 \rightleftharpoons 56 \rightleftharpoons 65, \tag{10}$$

ordered from smallest to largest extension change relative to unwrapped. The rate constants for transitions between states *i* and *j* at a force *F* have the form [56]:

$$k_{i\to j}(F) = k_0 \exp\left(-(\Delta G^{\ddagger} + \int_0^F \Delta x^{\ddagger}(F')dF')/k_BT\right),$$

where k_0 is the attempt rate over the barrier, $\Delta G^{\ddagger}$ is the barrier height at zero force, and $\Delta x^{\ddagger}$ is the distance between state *i* and the transition state between *i* and *j*. The integral in the exponential accounts for the effect of force on the barrier [56]. For $\Delta x^{\ddagger} > 0$, corresponding to a wrapping transition, the barrier increases with force and the rate decreases (conversely, for $\Delta x^{\ddagger} < 0$, corresponding to unwrapping, the barrier decreases and the rate increases). For example, the rate of wrapping from $(SSB)_{35}$ to $(SSB)_{56}$ is given by

$$k_{35\to 56}(F) = k_0 \exp\left(-\frac{(G^{\ddagger}_{35/56} - G_{35}) + \int_0^F (x^{\ddagger}_{35/56}(F') - x_{35}(F'))dF'}{k_BT}\right), \tag{11}$$

where G_{35} and x_{35} are the free energy and extension of the $(SSB)_{35}$ state and $G^{\ddagger}_{35/56}$ and $x^{\ddagger}_{35/56}$ are the free energy and extension of the transition state between the two wrapping states. The corresponding rate of unwrapping from $(SSB)_{56}$ to $(SSB)_{35}$ is

$$k_{56\to 35}(F) = k_0 \exp\left(-\frac{(G^{\ddagger}_{35/56} - G_{56}) - \int_0^F (x_{56}(F') - x^{\ddagger}_{35/56}(F'))dF'}{k_B T} \right). \quad (12)$$

Note that the equilibrium constant between the two states is

$$K^{eq}_{35\leftrightarrow 56}(F) = \frac{k_{35\to 56}(F)}{k_{56\to 35}(F)} = e^{-\left((G_{56}-G_{35}) + \int_0^F (x_{56}(F') - x_{35}(F'))dF'\right)/k_B T},$$

which matches Eq. (9), as expected.

According to the pathway (10), the lifetime of the *i*-th state is given by the rates out of that state:

$$\tau_i = \frac{1}{k_{i\to i+1} + k_{i\to i-1}}$$

In addition, the probabilities that the complex undergoes a transition from state *i* to *i*±1 are given by:

$$p_{i\to i\pm 1} = \frac{k_{i\to i\pm 1}}{k_{i\to i+1} + k_{i\to i-1}}$$

Both quantities were measured directly from the constant force experiments (**Figure 2**), and the individual wrapping and unwrapping rate constants were determined from the relation $k_{i\to i\pm 1} = p_{i\to i\pm 1} / \tau_i$ (**Figure 6-figure supplement 2**). To determine the barrier heights, we fitted these rates to expressions of the form Eqs. (11) and (12). We used a value of $k_0 \sim 10^7 \mathrm{s}^{-1}$ for the attempt rate, consistent with estimates based on Kramers' kinetic theory [57] and the range of values used in nucleosome unwrapping experiments [58] and protein and nucleic acid unfolding experiments [59, 60]. For simplicity, we assumed the transition state extensions $x^{\ddagger}_i$ were force-independent. In addition, we

used the values for the wrapping intermediate free energies G_i and extensions x_i obtained from analysis of the wrapping probabilities vs. force, as described in the previous section.

Thus, the data in **Figure 6-figure supplement 2** were fitted globally using six parameters: $G^{\ddagger}_{35/56}$ = –2.9 k_BT, $G^{\ddagger}_{17/35}$ = 6.9 k_BT, $G^{\ddagger}_{0/17}$ = 15 k_BT, measured relative to the unwrapped state energy G_0 = 0; and $x^{\ddagger}_{35/56}$ = 11.7 nm, $x^{\ddagger}_{17/35}$ = 6.4 nm, $x^{\ddagger}_{0/17}$ = 1.5 nm, measured relative to the unwrapped state extension x_0 = 0. We estimate the error in the barrier heights to be ~3 k_BT, due to the uncertainty in the attempt rate k_0. The spatial and temporal resolution of our measurement at forces ≤ 1 pN did not allow an accurate determination of the transition rates between $(SSB)_{65}$ and $(SSB)_{56}$ binding modes. Presumably, the transitions are too rapid to be detected. We estimated that the barrier between those two states must be <15 k_BT, based on the argument that intermediates lasting >0.3 s would be detected. The corresponding energy landscape is presented in **Figure 6**. The positions of the barriers were estimated to be roughly halfway between states based on the fact that the wrapping and unwrapping transitions between those states were equally force-dependent (**Figure 6-figure supplement 2**).

642 # ACKNOWLEDGEMENTS

643 We are grateful to Christopher Maffeo in the Aksimentiev Laboratory for helpful discussions. We thank
644 current and former members of the Chemla and Lohman Laboratories for providing help with
645 experiments.

646

647 The authors declare that they have no conflict of interest.

648

REFERENCES

1. Meyer, R.R. and P.S. Laine, *The single-stranded DNA-binding protein of Escherichia coli.* Microbiological Reviews, 1990. **54**: 342-380.
2. Shereda, R.D., A.G. Kozlov, T.M. Lohman, M.M. Cox, and J.L. Keck, *SSB as an organizer/mobilizer of genome maintenance complexes.* Crit Rev Biochem Mol Biol, 2008. **43**(5): 289-318. doi:10.1080/10409230802341296.
3. Lohman, T.M. and M.E. Ferrari, *Escherichia coli single-stranded DNA-binding protein: multiple DNA-binding modes and cooperativities.* Annu Rev Biochem, 1994. **63**: 527-70. doi:10.1146/annurev.bi.63.070194.002523.
4. Lohman, T.M. and L.B. Overman, *Two binding modes in Escherichia coli single strand binding protein-single stranded DNA complexes. Modulation by NaCl concentration.* J Biol Chem, 1985. **260**(6): 3594-603.
5. Raghunathan, S., A.G. Kozlov, T.M. Lohman, and G. Waksman, *Structure of the DNA binding domain of E-coli SSB bound to ssDNA.* Nature Structural Biology, 2000. **7**(8): 648-652. doi:10.1038/77943.
6. Raghunathan, S., C.S. Ricard, T.M. Lohman, and G. Waksman, *Crystal structure of the homo-tetrameric DNA binding domain of Escherichia coli single-stranded DNA-binding protein determined by multiwavelength x-ray diffraction on the selenomethionyl protein at 2.9-A resolution.* Proc Natl Acad Sci U S A, 1997. **94**(13): 6652-7.
7. Bujalowski, W. and T.M. Lohman, *Monomer-tetramer equilibrium of the Escherichia coli ssb-1 mutant single strand binding protein.* J Biol Chem, 1991. **266**(3): 1616-26.
8. Bujalowski, W. and T.M. Lohman, *Escherichia coli single-strand binding protein forms multiple, distinct complexes with single-stranded DNA.* Biochemistry, 1986. **25**(24): 7799-802. doi:10.1021/bi00372a003.
9. Lohman, T.M., L.B. Overman, and S. Datta, *Salt-dependent changes in the DNA binding co-operativity of Escherichia coli single strand binding protein.* J Mol Biol, 1986. **187**(4): 603-15. doi:10.1016/0022-2836(86)90338-4.
10. Ruyechan, W.T. and J.G. Wetmur, *Studies on the cooperative binding of the Escherichia coli DNA unwinding protein to single-stranded DNA.* Biochemistry, 1975. **14**(25): 5529-34. doi:10.1021/bi00696a023.
11. Sigal, N., H. Delius, T. Kornberg, M.L. Gefter, and B. Alberts, *A DNA-unwinding protein isolated from Escherichia coli: its interaction with DNA and with DNA polymerases.* Proc Natl Acad Sci U S A, 1972. **69**(12): 3537-41.
12. Kozlov, A.G., E. Weiland, A. Mittal, V. Waldman, E. Antony, N. Fazio, R.V. Pappu, and T.M. Lohman, *Intrinsically disordered C-terminal tails of E. coli single-stranded DNA binding protein regulate cooperative binding to single-stranded DNA.* J Mol Biol, 2015. **427**(4): 763-74. doi:10.1016/j.jmb.2014.12.020.
13. Lohman, T.M., W. Bujalowski, and L.B. Overman, *E. coli single strand binding protein: a new look at helix-destabilizing proteins.* Trends Biochem Sci, 1988. **13**(7): 250-5.
14. Wessel, S.R., A.H. Marceau, S.C. Massoni, R. Zhou, T. Ha, S.J. Sandler, and J.L. Keck, *PriC-mediated DNA replication restart requires PriC complex formation with the single-stranded DNA-binding protein.* J Biol Chem, 2013. **288**(24): 17569-78. doi:10.1074/jbc.M113.478156.
15. Bhattacharyya, B., N.P. George, T.M. Thurmes, R. Zhou, N. Jani, S.R. Wessel, S.J. Sandler, T. Ha, and J.L. Keck, *Structural mechanisms of PriA-mediated DNA replication restart.* Proc Natl Acad Sci U S A, 2014. **111**(4): 1373-8. doi:10.1073/pnas.1318001111.

16. Chrysogelos, S. and J. Griffith, *Escherichia coli single-strand binding protein organizes single-stranded DNA in nucleosome-like units.* Proc Natl Acad Sci U S A, 1982. **79**(19): 5803-7.
17. Griffith, J.D., L.D. Harris, and J. Register, 3rd, *Visualization of SSB-ssDNA complexes active in the assembly of stable RecA-DNA filaments.* Cold Spring Harb Symp Quant Biol, 1984. **49**: 553-9. doi:10.1101/SQB.1984.049.01.062.
18. Bujalowski, W. and T.M. Lohman, *Negative co-operativity in Escherichia coli single strand binding protein-oligonucleotide interactions. II. Salt, temperature and oligonucleotide length effects.* J Mol Biol, 1989. **207**(1): 269-88. doi:10.1016/0022-2836(89)90455-5.
19. Bujalowski, W. and T.M. Lohman, *Negative co-operativity in Escherichia coli single strand binding protein-oligonucleotide interactions. I. Evidence and a quantitative model.* J Mol Biol, 1989. **207**(1): 249-68. doi:10.1016/0022-2836(89)90454-3.
20. Bujalowski, W., L.B. Overman, and T.M. Lohman, *Binding mode transitions of Escherichia coli single strand binding protein-single-stranded DNA complexes. Cation, anion, pH, and binding density effects.* J Biol Chem, 1988. **263**(10): 4629-40.
21. Roy, R., A.G. Kozlov, T.M. Lohman, and T. Ha, *Dynamic Structural Rearrangements Between DNA Binding Modes of E. coli SSB Protein.* J Mol Biol, 2007. **369**(5): 1244-57. doi:10.1016/j.jmb.2007.03.079.
22. Roy, R., A.G. Kozlov, T.M. Lohman, and T. Ha, *SSB protein diffusion on single-stranded DNA stimulates RecA filament formation.* Nature, 2009. **461**(7267): 1092-7. doi:10.1038/nature08442.
23. Zhou, R., A.G. Kozlov, R. Roy, J. Zhang, S. Korolev, T.M. Lohman, and T. Ha, *SSB functions as a sliding platform that migrates on DNA via reptation.* Cell, 2011. **146**(2): 222-32. doi:10.1016/j.cell.2011.06.036.
24. Pant, K., R.L. Karpel, I. Rouzina, and M.C. Williams, *Salt dependent binding of T4 gene 32 protein to single and double-stranded DNA: single molecule force spectroscopy measurements.* J Mol Biol, 2005. **349**(2): 317-30. doi:10.1016/j.jmb.2005.03.065.
25. Shokri, L., B. Marintcheva, C.C. Richardson, I. Rouzina, and M.C. Williams, *Single Molecule Force Spectroscopy of Salt-dependent Bacteriophage T7 Gene 2.5 Protein Binding to Single-stranded DNA.* J. Biol. Chem., 2006. **281**(50): 38689-38696. doi:10.1074/jbc.M608460200.
26. Hatch, K., C. Danilowicz, V. Coljee, and M. Prentiss, *Direct measurements of the stabilization of single-stranded DNA under tension by single-stranded binding proteins.* Phys Rev E Stat Nonlin Soft Matter Phys, 2007. **76**(2 Pt 1): 021916. doi:10.1103/PhysRevE.76.021916.
27. Hatch, K., C. Danilowicz, V. Coljee, and M. Prentiss, *Measurement of the salt-dependent stabilization of partially open DNA by Escherichia coli SSB protein.* Nucleic Acids Res, 2008. **36**(1): 294-9. doi:10.1093/nar/gkm1014.
28. Bustamante, C., J.F. Marko, E.D. Siggia, and S. Smith, *Entropic elasticity of lambda-phage DNA.* Science, 1994. **265**(5178): 1599-600. doi:10.1126/science.8079175.
29. Saleh, O.A., D.B. McIntosh, P. Pincus, and N. Ribeck, *Nonlinear low-force elasticity of single-stranded DNA molecules.* Phys Rev Lett, 2009. **102**(6): 068301. doi:10.1103/PhysRevLett.102.068301.
30. Comstock, M.J., T. Ha, and Y.R. Chemla, *Ultrahigh-resolution optical trap with single-fluorophore sensitivity.* Nat Methods, 2011. **8**(4): 335-40. doi:10.1038/nmeth.1574.
31. Neuman, K.C. and S.M. Block, *Optical trapping.* Rev Sci Instrum, 2004. **75**(9): 2787-809. doi:10.1063/1.1785844.
32. Gao, Y., S. Zorman, G. Gundersen, Z. Xi, L. Ma, G. Sirinakis, J.E. Rothman, and Y. Zhang, *Single reconstituted neuronal SNARE complexes zipper in three distinct stages.* Science, 2012. **337**(6100): 1340-3. doi:10.1126/science.1224492.

33. Khamis, M.I., J.R. Casas-Finet, A.H. Maki, J.B. Murphy, and J.W. Chase, *Role of tryptophan 54 in the binding of E. coli single-stranded DNA-binding protein to single-stranded polynucleotides.* FEBS Lett, 1987. **211**(2): 155-9. doi:10.1016/0014-5793(87)81427-8.
34. Casas-Finet, J.R., M.I. Khamis, A.H. Maki, and J.W. Chase, *Tryptophan 54 and phenylalanine 60 are involved synergistically in the binding of E. coli SSB protein to single-stranded polynucleotides.* FEBS Lett, 1987. **220**(2): 347-52. doi:10.1016/0014-5793(87)80844-X.
35. Ferrari, M.E., J. Fang, and T.M. Lohman, *A mutation in E. coli SSB protein (W54S) alters intra-tetramer negative cooperativity and inter-tetramer positive cooperativity for single-stranded DNA binding.* Biophys Chem, 1997. **64**(1-3): 235-51.
36. Maffeo, C., *Quantitative all-atom and coarse-grained molecular dynamics simulation studies of DNA*, in *Doctoral Dissertation*. 2015, University of Illinois at Urbana-Champaign,
37. Forster, T., **Zwischenmolekulare Energiewanderung Und Fluoreszenz.* Annalen Der Physik, 1948. **2**(1-2): 55-75.
38. Romer, R., U. Schomburg, G. Krauss, and G. Maass, *The E. coli single-stranded DNA binding protein is mobile on DNA: ^{1}H-NMR study of its interaction with oligo- and polynucleotides.* Biochem., 1984. **23**: 6132-6137.
39. Bujalowski, W. and T.M. Lohman, *Monomers of the Escherichia coli SSB-1 mutant protein bind single-stranded DNA.* J Mol Biol, 1991. **217**(1): 63-74. doi:10.1016/0022-2836(91)90611-9.
40. Krauss, G., H. Sindermann, U. Schomburg, and G. Maass, *Escherichia coli single-strand deoxyribonucleic acid binding protein: stability, specificity, and kinetics of complexes with oligonucleotides and deoxyribonucleic acid.* Biochemistry, 1981. **20**(18): 5346-52. doi:10.1021/bi00521a040.
41. Hegner, M., S.B. Smith, and C. Bustamante, *Polymerization and mechanical properties of single RecA-DNA filaments.* Proc Natl Acad Sci U S A, 1999. **96**(18): 10109-14. doi:10.1073/pnas.96.18.10109.
42. Galletto, R., I. Amitani, R.J. Baskin, and S.C. Kowalczykowski, *Direct observation of individual RecA filaments assembling on single DNA molecules.* Nature, 2006. **443**(7113): 875-8. doi:10.1038/nature05197.
43. Bell, J.C., J.L. Plank, C.C. Dombrowski, and S.C. Kowalczykowski, *Direct imaging of RecA nucleation and growth on single molecules of SSB-coated ssDNA.* Nature, 2012. **491**(7423): 274-8. doi:10.1038/nature11598.
44. Joo, C., S.A. McKinney, M. Nakamura, I. Rasnik, S. Myong, and T. Ha, *Real-time observation of RecA filament dynamics with single monomer resolution.* Cell, 2006. **126**(3): 515-27. doi:10.1016/j.cell.2006.06.042.
45. Nguyen, B., J. Sokoloski, R. Galletto, E.L. Elson, M.S. Wold, and T.M. Lohman, *Diffusion of human replication protein A along single-stranded DNA.* J Mol Biol, 2014. **426**(19): 3246-61. doi:10.1016/j.jmb.2014.07.014.
46. Sancar, A., K.R. Williams, J.W. Chase, and W.D. Rupp, *Sequences of the ssb gene and protein.* Proc Natl Acad Sci U S A, 1981. **78**(7): 4274-8.
47. Lohman, T.M., J.M. Green, and R.S. Beyer, *Large-scale overproduction and rapid purification of the Escherichia coli ssb gene product. Expression of the ssb gene under lambda PL control.* Biochemistry, 1986. **25**(1): 21-5. doi:10.1021/bi00349a004.
48. Brewer, L.R. and P.R. Bianco, *Laminar flow cells for single-molecule studies of DNA-protein interactions.* Nat Methods, 2008. **5**(6): 517-25. doi:10.1038/nmeth.1217.
49. Landry, M.P., P.M. McCall, Z. Qi, and Y.R. Chemla, *Characterization of photoactivated singlet oxygen damage in single-molecule optical trap experiments.* Biophys J, 2009. **97**(8): 2128-36. doi:10.1016/j.bpj.2009.07.048.

50. Rasnik, I., S.A. McKinney, and T. Ha, *Nonblinking and long-lasting single-molecule fluorescence imaging.* Nat Methods, 2006. **3**(11): 891-3. doi:10.1038/nmeth934.
51. Wei, T.F., W. Bujalowski, and T.M. Lohman, *Cooperative binding of polyamines induces the Escherichia coli single-strand binding protein-DNA binding mode transitions.* Biochemistry, 1992. **31**(26): 6166-74. doi:10.1021/bi00141a029.
52. Baumann, C.G., S.B. Smith, V.A. Bloomfield, and C. Bustamante, *Ionic effects on the elasticity of single DNA molecules.* Proc Natl Acad Sci U S A, 1997. **94**(12): 6185-90.
53. Langevin, P., *Magnetism and theory of electrons.* Annales De Chimie Et De Physique, 1905. **5**: 70-127.
54. Chen, H., G. Yuan, R.S. Winardhi, M. Yao, I. Popa, J.M. Fernandez, and J. Yan, *Dynamics of equilibrium folding and unfolding transitions of titin immunoglobulin domain under constant forces.* J Am Chem Soc, 2015. **137**(10): 3540-6. doi:10.1021/ja5119368.
55. Bustamante, C., Y.R. Chemla, N.R. Forde, and D. Izhaky, *Mechanical processes in biochemistry.* Annu Rev Biochem, 2004. **73**: 705-48. doi:10.1146/annurev.biochem.72.121801.161542.
56. Dudko, O.K., G. Hummer, and A. Szabo, *Theory, analysis, and interpretation of single-molecule force spectroscopy experiments.* Proc Natl Acad Sci U S A, 2008. **105**(41): 15755-60. doi:10.1073/pnas.0806085105.
57. Kramers, H.A., *Brownian motion in a field of force and the diffusion model of chemical reactions.* Physica, 1940. **7**: 284-304. doi:Doi 10.1016/S0031-8914(40)90098-2.
58. Pope, L.H., M.L. Bennink, K.A. van Leijenhorst-Groener, D. Nikova, J. Greve, and J.F. Marko, *Single chromatin fiber stretching reveals physically distinct populations of disassembly events.* Biophys J, 2005. **88**(5): 3572-83. doi:10.1529/biophysj.104.053074.
59. Yang, W.Y. and M. Gruebele, *Folding at the speed limit.* Nature, 2003. **423**(6936): 193-7. doi:10.1038/nature01609.
60. Woodside, M.T., W.M. Behnke-Parks, K. Larizadeh, K. Travers, D. Herschlag, and S.M. Block, *Nanomechanical measurements of the sequence-dependent folding landscapes of single nucleic acid hairpins.* Proc Natl Acad Sci U S A, 2006. **103**(16): 6190-5. doi:10.1073/pnas.0511048103.

FIGURE CAPTIONS

Figure 1. Unwrapping of ssDNA from *E. coli* SSB under mechanical tension. (**A**) Crystal structure (Protein Data Bank ID number 1EYG) and schematic representation of an *E. coli* SSB tetramer wrapped by 70 nt of ssDNA (blue) in the $(SSB)_{65}$ mode. From 5' to 3', ssDNA interacts with the yellow, purple, green and red subunits. (**B**) Schematic of SSB unwrapping experiment. A DNA construct consisting of two long dsDNA handles and a short $(dT)_{70}$ ssDNA site is tethered between two optically trapped beads in the absence of SSB (Position 1, panel C). When moved to the stream containing SSB (Position 2), a single SSB tetramer binds to the ssDNA site at low tension (~0.5 pN). The tethered DNA is moved back to the blank stream (Position 1) and a ramping force is applied. Stretching the nucleoprotein complex to >20 pN causes the SSB to dissociate. (**C**) Experimental flow chamber. Two separate streams containing experimental buffer only (red, Position 1) and buffer plus 0.5 nM SSB (blue, Position 2) form a laminar interface with minimal mixing. (**D**) Representative force-extension curves. Relaxing curves (red) are obtained after SSB dissociation, and are well fit to a polymer model of bare DNA (black dotted line, Materials and Methods). Stretching curves (purple) of the SSB-ssDNA complex deviate from a model assuming the protein adopts the $(SSB)_{65}$ wrapping mode at all forces (black dashed line). Cartoon illustration of SSB unwrapping shows the SSB behavior at particular forces. (**E**) Change in extension upon SSB wrapping vs. applied force. The change in extension is determined from the extension difference between stretching and relaxing curves in (D). Individual traces (gray) are binned and averaged to yield a mean change in extension (black opened circle; error bars are S.D.). The data deviates from the model (dashed line, determined from the difference between the dashed and dotted lines in (D)) at forces >1 pN. Representative traces (red, green, and blue) display the differences between the individual and averaged traces.

Figure 2. Intermediate ssDNA wrapping states of SSB under tension. (**A**) Schematic of SSB constant force wrapping experiment. A DNA construct is held between two optical traps under a constant tension between 2-10 pN in the presence of protein. An extension change, Δx, is measured upon SSB binding, wrapping or unwrapping ssDNA. At the end of each observation, SSB is removed by stretching the DNA construct to high force (>20 pN). (**B**) Representative time traces of SSB-ssDNA wrapping at 2, 5, 7, and 9 pN (red, green, blue, and purple respectively). Extension change data were acquired at 66 kHz and boxcar averaged to 10 Hz (dark color). In all traces, SSB first binds and compacts ssDNA as indicated by an extension decrease. Depending on tension, SSB displays several intermediate wrapping states. Black dashed lines represent the mean extension change of each particular wrapping state. (**C**) Extension change distribution from many SSB wrapping traces at constant tensions between 2-10 pN. The color map matches that in (B). Solid lines are multi-Gaussian fits to the distributions.

Figure 3. SSB wrapping modes. (**A**) Mean change in extension Δx vs. tension for each wrapping state, derived from the peaks of the distributions in **Figure 2C**. Error bars represent S.E.M. and were determined by bootstrapping. The dashed line is the model in **Figure 1D**. Solid lines represent models of Δx based on Eq. (3) for SSB wrapping N_w = 65, 56, 35, and ~17 nt (purple, blue, green, and red, respectively; Materials and Methods). Data points are clustered into 4 groups corresponding to those states (purple, blue, green, and red circles). (**B**) Schematic representation of Δx. Top: Bare ssDNA (with N_{ss} = 70 nt) and its extension, x_{bare}, based on a polymer elasticity model Eq. (1) (Materials and Methods). Bottom: SSB-wrapped ssDNA showing the number of wrapped nucleotides, N_w (<70, red) and the remaining unwrapped nucleotides ($N_{ss} - N_w$, blue). The extension of wrapped DNA, x_{wrap} is calculated from an elasticity model and the effective physical size of the SSB-ssDNA complex, x_{SSB}^{eff}, Eq. (2) (Materials and Methods). Δx is the difference between x_{wrap} and x_{bare}, Eq. (3). (**C**) Number of

wrapped nucleotides N_w vs. tension *F*. Each data point in (**A**) is mapped to N_w using the model described in the text (Materials and Methods; **Figure 3-figure supplement 1**). Dotted lines represent the maximum possible range of N_w for each colored group of points based on x_{SSB}^{eff} being <6.5 nm (**Figure 3-figure supplement 1**, left panel). Dashed lines represent a tighter range of possible N_w for each group of points derived from the SSB-ssDNA structure (**Figure 3-figure supplement 1**, middle panel). Error bars represent this range for each individual data point. The shaded areas represent the tightest range of possible N_w for each group based on the 'hotspot' analysis described in the text (**Figure 3-figure supplement 1**, right panel). The points are the best estimates of N_w from the model. The shaded areas and solid lines in (**C**) map directly to those in (**A**). Cartoon schematics depict possible wrapping modes corresponding to the 4 groups.

Figure 4. SSB binding modes and diffusion mechanism. (**A**) Schematic of fluorescently labeled SSB, SSB_f, ssDNA wrapping experiment. A Cy5-labeled DNA construct is tethered between two optical traps under a constant tension of 5 pN. Upon binding of an AlexaFluor555-labeled SSB, both DNA extension change, Δx, and smFRET are measured simultaneously. (**B**) Scatter plot of FRET efficiency and Δx. Data (circles) are assigned to 4 states (red (i), blue (ii), black (iii), and green (iv)) based on the value of FRET and Δx. A density map of the combined FRET-extension states overlaid with the scatter plot confirms that the data can be separated into 4 states. Cartoon illustrations of nucleoprotein complexes demonstrate possible SSB wrapping configurations corresponding to the 4 assigned states. (**C**) Representative traces showing combined fluorescence and DNA extension measurements. Change in extension (top; boxcar averaged to 50 Hz) and fluorescence (middle; boxcar averaged to 0.5 Hz) of donor (SSB_f, green) and acceptor (Cy5, red) are measured simultaneously. Together, FRET efficiency (bottom; blue) and extension change (top;

884 black) reveal the SSB wrapping states (i & ii, iii & iv) and their dynamics (ssDNA wrapping/releasing and
885 sliding).

886

887 **Figure 5. Unwrapping of ssDNA from SSB by RecA filament formation.** (**A**) Schematic representation of
888 SSB-RecA experiment. A standard DNA construct consisting of a 70-nt single-stranded DNA ($(dT)_{70}$)
889 fragment was synthesized to contain two internal 18-atom hexa-ethylene-glycol spacers at both ss-
890 dsDNA junctions (cyan; Materials and Methods). The spacers prevent RecA filament formation onto the
891 dsDNA. The construct is tethered in the presence of SSB. After the SSB binds, the tethered DNA is
892 moved to the stream containing RecA for observation. (**B**) Experimental flow chamber for SSB-RecA
893 experiment. Two separate streams contain experimental buffer plus 0.5 nM SSB (red, Position 1) and
894 buffer plus 125 nM RecA and 125 μM ATP-γS (blue, Position 2). (**C**) Representative time traces showing
895 competition between RecA and SSB on ssDNA (green, blue, red). Transient wrapping-unwrapping of SSB
896 slows down the nucleation of RecA. Formation of RecA filament extends ssDNA (blue box), displaces the
897 SSB, and stops after reaching the spacers at the ss-dsDNA junctions. The dotted lines correspond to the
898 model in (**D**). (**D**) Extension change distribution of SSB-RecA intermediates at a constant tension of 5 pN
899 (pink) obtained from many RecA filament formation time traces (N = 25). Five states representing SSB-
900 RecA dissociation intermediates are illustrated (schematics) and assigned to peaks of the distribution.
901 Extensions corresponding to these states are predicted using polymer models of elasticity (black dots
902 and dotted lines, Material and Methods).

903

904 **Figure 6. Energy landscape of SSB wrapping.** Energy landscapes of a single SSB wrapping ssDNA at
905 representative forces reconstructed from extension change probability distributions vs. tension (**Figure**
906 **2C**). The potential wells correspond to the stable SSB-ssDNA intermediates (cartoon schematics): $(SSB)_{65}$,

907 $(SSB)_{56}$, $(SSB)_{35}$, $(SSB)_{17}$, and unbound, respectively. The energy associated with each intermediate is
908 determined from the occurrence probabilities for each state (squares, Material and Methods). The
909 barrier heights and positions (circles) are determined from the state lifetimes (Materials and Methods).
910 In the absence of tension, SSB wraps ssDNA in the $(SSB)_{65}$ binding mode. Increasing tension (brown,
911 orange, cyan, purple lines correspond to 0, 3, 7, 9 pN, respectively) tilts the energy landscape, changes
912 the free-energy difference between wrapping intermediates, and favors different SSB-ssDNA binding
913 modes.

914

SUPPORTING FIGURE CAPTIONS

Figure 1-figure supplement 1. Dissociation of SSB upon DNA stretching. Averaged stretching (blue) and relaxing (red) FEC from **Figure 1D**, and bare DNA FEC (green). Both the relaxing and bare DNA stretching curves are fitted to the polymer elasticity model with 3,260 bp dsDNA handles and 70 nt ssDNA (black dashed line, Material and Methods). The model assumes zero extension at zero force and fits the data. The resulting fits are consistent with each other, indicating that SSB has dissociated during stretching. Error bars are S.D.

Figure 1-figure supplement 2. Single-stranded DNA polymer modeling. Representative force-extension curves (FEC) of stretching and relaxing a DNA construct containing 3,260 bp dsDNA handles and 70 nt (green) or 140 nt (orange) ssDNA. The total extension of the tether is modeled by the sum of dsDNA and ssDNA extensions. The dsDNA segment is modeled using the extensible worm-liked chain (XWLC), while the ssDNA segment is fitted to the snake-like chain (SLC; Materials and Methods). Black dashed and dotted lines are fits to the 70 nt and 140 nt ssDNA constructs, respectively. The extension difference (inset, blue) between 70 nt and 140 nt ssDNA constructs illustrates the validity of the ssDNA elasticity model over short lengths (70 nt).

Figure 1-figure supplement 3. Dissociation force of SSB-ssDNA. Cartoon schematic and representative traces showing combined fluorescence and DNA extension measurements. A DNA construct bound by fluorescently labeled SSB, SSB_f, is stretched (blue) and relaxed (red) under mechanical force. Upon reaching a force ~10 pN, SSB_f dissociates from the DNA as indicated by the decrease in fluorescence. The relaxing curves from the corresponding force-extension curves match the polymer elasticity model of bare DNA (black dotted line, Material and Methods) indicating that the SSB has dissociated during stretching. The dissociation force from the FECs is consistent with the fluorescence data.

Figure 1-figure supplement 4. Sample chamber. Image and schematic of a laminar flow chamber. Two glass coverslips are used to sandwich patterned parafilm (Nescofilm). For illustration purposes, food dye of different colors is flowed into the chamber via inlet tubing at a rate of 100 µl/hr. Two streams, one containing experimental buffer only (red, 1), and the other containing buffer plus SSB (blue, 2), merge into the central channel but do not mix appreciably due to the laminar flow. The chamber design allows rapid exchange of buffer conditions by moving the optical traps across the stream interface. The top channel (yellow) is loaded with anti-digoxigenin beads, while the bottom channel (green) is loaded with DNA-bound streptavidin beads. Both beads diffuse through glass capillaries into the middle channel where the optical trapping experiment is performed.

Figure 1-figure supplement 5. DNA construct. Schematic of single-stranded DNA construct. The DNA construct consists of three separate fragments ligated together (Materials and Methods): 'Right Handle' (RH), 'Left Handle' (LH), and 'Binding Site' (BS). The handles served as functionalized linkers that connect to trapped beads through biotin-streptavidin and digoxigenin-anti-digoxigenin linkages and spatially separate the beads from the protein binding site.

Figure 1-figure supplement 6. SSB binds to dT_{70} in the fully wrapped $(SSB)_{65}$ mode at a 1:1 molar ratio in 100 mM Tris buffer. Results of an equilibrium titration of Cy5-$(dT)_{70}$-Cy3-dT-3' (0.1 µM) with SSB (left panel; 100 mM Tris-HCl, 20 mM NaCl, 0.1mM EDTA, 25°C) plotted as normalized Cy5 fluorescence (F_n = $(F - F_0)/F_0$) versus molar ratio of total SSB protein (tetramer) to total DNA concentrations (where F_0 is the fluorescence intensity of DNA alone and F is the fluorescence measured at each point in the titration). The biphasic character of the binding isotherm indicates that two types of complexes can form, the first having one and the second having two tetramers bound and characterized by high and

963 intermediate FRET values ($(SSB)_{65}$ and $(SSB)_{35}$ modes, respectively). The continuous line represents the
964 best fit to the data based on a two-site model [22] with equilibrium binding constants, $k_1 = 1\times10^{10}$ M^{-1}
965 (minimum estimate) and $k_2 = (1.21\pm0.04)\times10^{8}$ M^{-1} and two additional parameters $F_1 = 10.1\pm0.1$ and $F_2 =$
966 4.8±0.1, reflecting the maximum Cy5 fluorescence observed for one and two tetramers bound,
967 respectively. Species distribution predicted from the best fit parameters listed above (right panel). At
968 low concentration of SSB tetramers the protein binds to dT_{70} exclusively in the fully wrapped $(SSB)_{65}$
969 binding mode, although as the SSB concentration increases ($[SSB]_{tot}/[dT_{70}]_{tot} > 1$) the $(SSB)_{35}$ binding
970 mode starts to form in which two SSB tetramers are bound to one molecule of dT_{70}.
971
972 **Figure 2-figure supplement 1. Single SSB binding and wrapping transitions.** Schematic and
973 representative traces illustrating a wrapping experiment with fluorescently labeled SSB, SSB_f. A DNA
974 construct is held between two optical traps at a constant tension of 2, 5, and 9 pN (left, middle, and
975 right panels). An extension change, Δx, is measured upon SSB_f wrapping or unwrapping ssDNA. Upon
976 SSB_f binding, a decrease in extension (gray) and increase in fluorescence (green) are observed
977 simultaneously (all panels). A further decrease in extension (middle panel) does not result in further
978 increase in fluorescence, indicating that the same SSB wraps additional ssDNA. At high forces (right
979 panel) extension increases correspond to SSB dissociation.
980
981 **Figure 3-figure supplement 1. SSB wrapping models.** Three-level modeling of SSB wrapping
982 configurations. Schematics of SSB, wrapped ssDNA (blue), and the distance between wrapped ends,
983 x_{SSB} (black arrow; top panels). Each extension change data point $\Delta x(F)$ in **Figure 3A** corresponds to a
984 curve in the space of possible N_w and x_{SSB}, according to Eq. (5) (colored curves, bottom panels). The
985 widths of the curves correspond to the error bars in **Figure 3A**. Selected data points from **Figure 3A** are

displayed (purple: *F* = 0.8 pN, Δ*x* = 11 nm, blue: 4 pN, 14 nm, green: 7 pN, 10 nm, and red: 9 pN, 7 nm). At the first level of modeling (left panels), x_{SSB} is assumed to be limited only by the size of the protein (i.e. x_{SSB} < 6.5 nm; dark gray shaded area). The range of possible N_w corresponding to each selected data point is shown by the colored dotted lines. At the second level (middle), the range of possible x_{SSB} is refined by utilizing the $(SSB)_{65}$ crystal structure. The end-to-end distance between every pair of nucleotides n_i and n_j along the ssDNA in the structural model defines a lower and upper bound of x_{SSB} for each N_w (gray shaded area). This, in turn, narrows down the range of possible N_w for each data point (colored dashed lines). At the third level (right), four 'hotspots', residues on each SSB monomer with which nucleotides interact most strongly (green molecular surfaces in the schematic and green nucleotides), are used to refine the estimates for x_{SSB} further. Three regions near the hotspots (black contours) are identified and used to calculate x_{SSB}. The numbering (1, 2, and 3) corresponds to the configurations shown in **Figure 3-figure supplement 2**. This analysis provides the narrowest estimate for the range of N_w for each data point Δx (colored bands). The best estimates for N_w are obtained from the center of this range (black dots); these are plotted in **Figure 3C** vs. force.

Figure 3-figure supplement 2. SSB wrapping pathway. Crystal structures and schematics of SSB wrapping ssDNA (blue) in different wrapping modes. Each mode illustrates possible wrapping configurations that correspond to the regions, numbered 1, 2, and 3 in **Figure 3-figure supplement 1**. As tension increases (from left to right), SSB wraps less ssDNA, and the number of hotspots interacting with ssDNA (green molecular surfaces in structures, black dots in schematics) decreases.

Figure 3-figure supplement 3. Wrapping modes of SSB mutant. Schematic of wrapping experiment using SSB_m, a SSB mutant in which Trp-54 is replaced by Ser-54. Comparison of extension change

distributions between wild-type SSB (left panels) and SSB_m (right). At the same tensions (3-5 pN), SSB_m wraps less ssDNA than wild-type SSB, and is more likely to wrap 35 nt. The mean number of wrapped nucleotides vs. tension was estimated in the same way as for wt SSB (**Figure 3C**).

Figure 4-figure supplement 1. Mechanism of SSB Diffusion. Cartoon illustrations of nucleoprotein complexes diffusing along ssDNA with different proposed mechanisms. Schematic FRET efficiency and Δx displaying multiple transitions between states (i, ii, iii, iv). In a sliding or reptation mechanism, FRET transitions occur independently of changes in wrapping state (top panel). A rolling mechanism involves SSB displacement by wrapping one end of DNA followed by releasing the other (bottom panel; i -> iii -> ii or ii -> iii -> i). No examples (0 of *N* = 82) of rolling are observed in our experiment.

Figure 5-figure supplement 1. RecA filament formation on modified single-stranded DNA. Schematics and representative time traces showing RecA filament formation experiment. A DNA construct consisting of two long dsDNA handles, a short 70-nt ssDNA site, and two spacers (cyan, Material and Methods) is held between two optical traps at a constant tension of 5 pN in the blank buffer. The construct is then moved into the buffer stream containing 125 nM RecA and 125 μM ATP-γS. A change in extension, Δx, is measured while RecA polymerizes, extending the ssDNA. Upon reaching the spacers, RecA filament formation stalls. The extension change distribution from many RecA filament formation time traces (blue, black, green; *N* = 22) are consistent with the polymer elasticity model of bare DNA and RecA-filled DNA (black dots; Materials and Methods), indicating that RecA has fully polymerized on ssDNA.

Figure 6-figure supplement 1. Occurrence probability of SSB wrapping intermediates. Extension change distributions (left panels) of many SSB wrapping events obtained from force-ramp experiments (1 pN) and constant force experiments (2-10 pN). Individual wrapping intermediates are analyzed and assigned to corresponding SSB binding modes based on **Figure 3C**. At all tensions, the probability of each SSB binding modes (right panels, color bars) is derived from the area under the distributions. The model (black circles, Material and Methods) obtained from the energy landscape in **Figure 6** matches well with the experimentally derived probabilities.

Figure 6-figure supplement 2. Modeling of transition rates between SSB wrapping intermediates. Unwrapping (solid circles) and wrapping (open squares) transition rates between different SSB wrapping intermediates vs. force. The rates were determined from dwell times and transition probabilities in **Figure 2C** (Materials and Methods). The data were fit globally (unwrapping, dashed line; wrapping, dotted line) using expressions of the form Eq. (11) and (12) using as parameters the three barriers and distances to the transition state $G^{\ddagger}_{35/56}$, $G^{\ddagger}_{17/35}$, $G^{\ddagger}_{0/17}$, $x^{\ddagger}_{35/56}$, $x^{\ddagger}_{17/35}$, and $x^{\ddagger}_{0/17}$ (Materials and Methods).

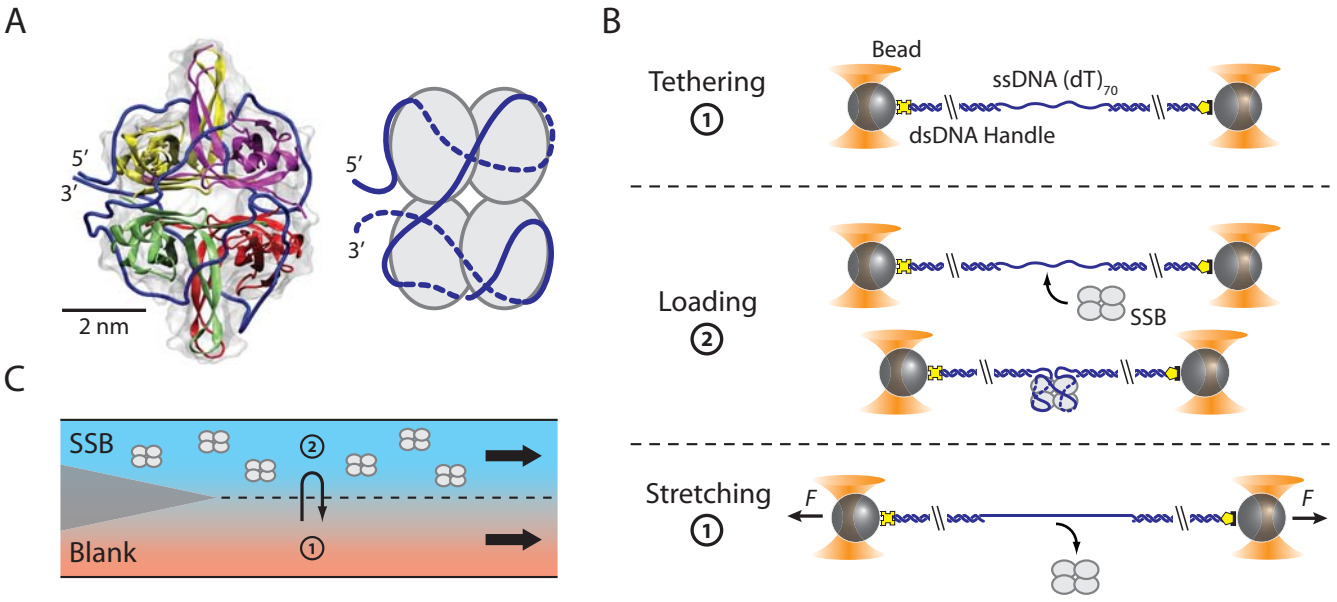
A
5′
3′
2 nm
5′
3′
B
Tethering
1
Bead
ssDNA (dT)70
dsDNA Handle
Loading
2
SSB
Stretching
1
F
F
C
SSB
2
1
Blank

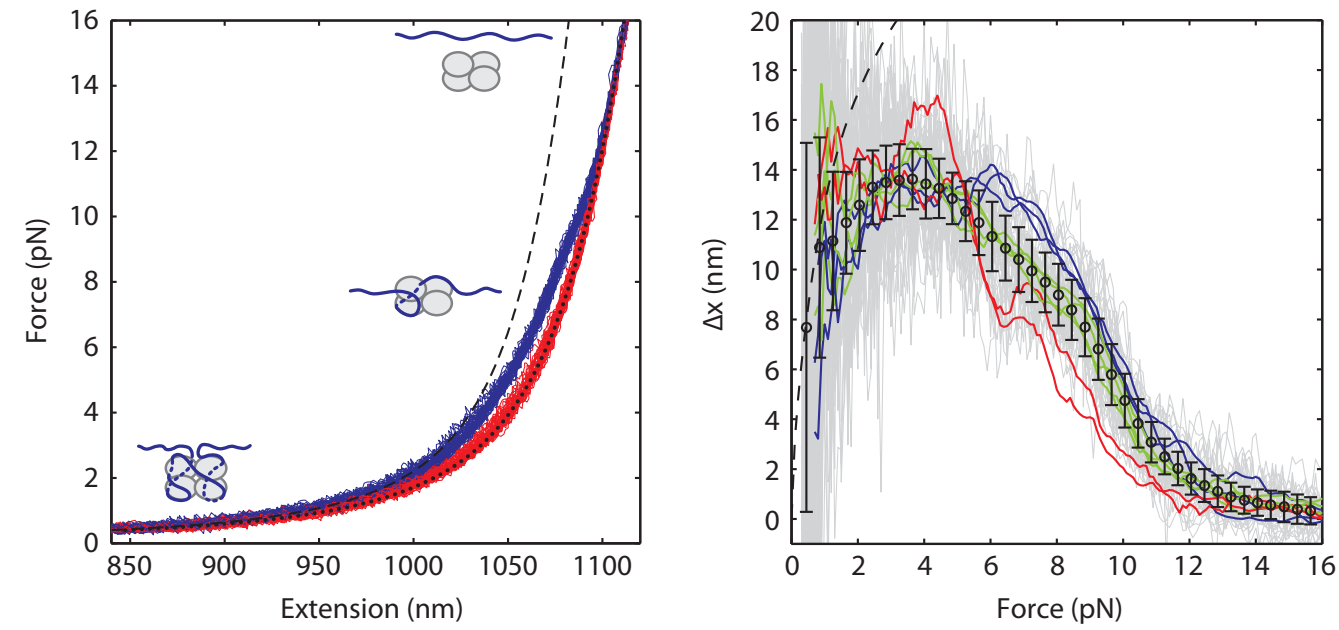
D
Force (pN)
Extension (nm)
0
2
4
6
8
10
12
14
16
850
900
950
1000
1050
1100
E
Δx (nm)
Force (pN)
0
2
4
6
8
10
12
14
16
18
20

Figure 1

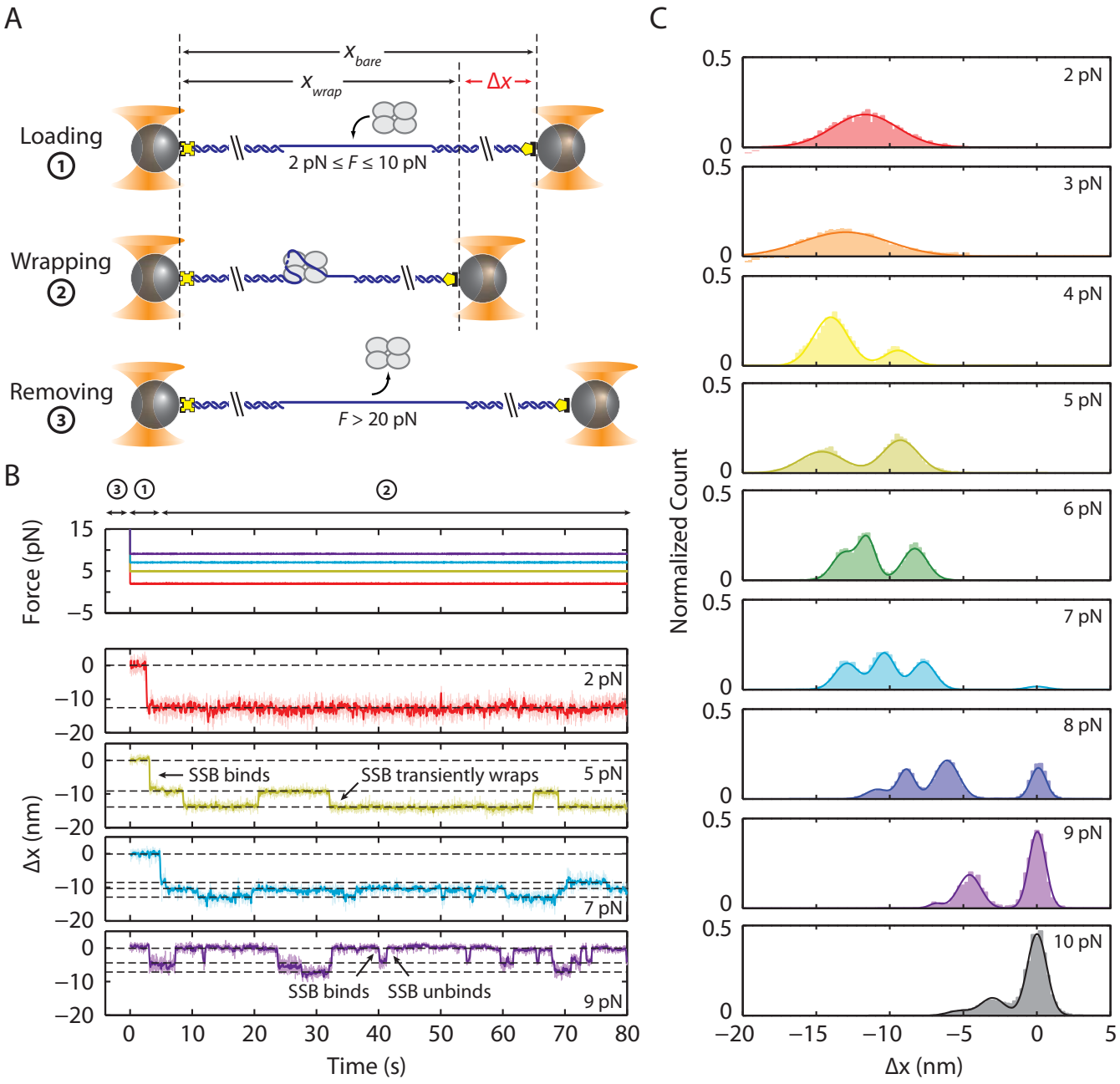
A
x_{bare}
x_{wrap}
Δx
Loading
1
2 pN ≤ F ≤ 10 pN
Wrapping
2
Removing
3
F > 20 pN
B
3 1
2
Force (pN)
15
5
−5
2 pN
5 pN
7 pN
9 pN
SSB binds
SSB transiently wraps
SSB binds
SSB unbinds
Δx (nm)
0
−10
−20
0 10 20 30 40 50 60 70 80
Time (s)
C
Normalized Count
0.5
0
2 pN
3 pN
4 pN
5 pN
6 pN
7 pN
8 pN
9 pN
10 pN
−20 −15 −10 −5 0 5
Δx (nm)

Figure 2

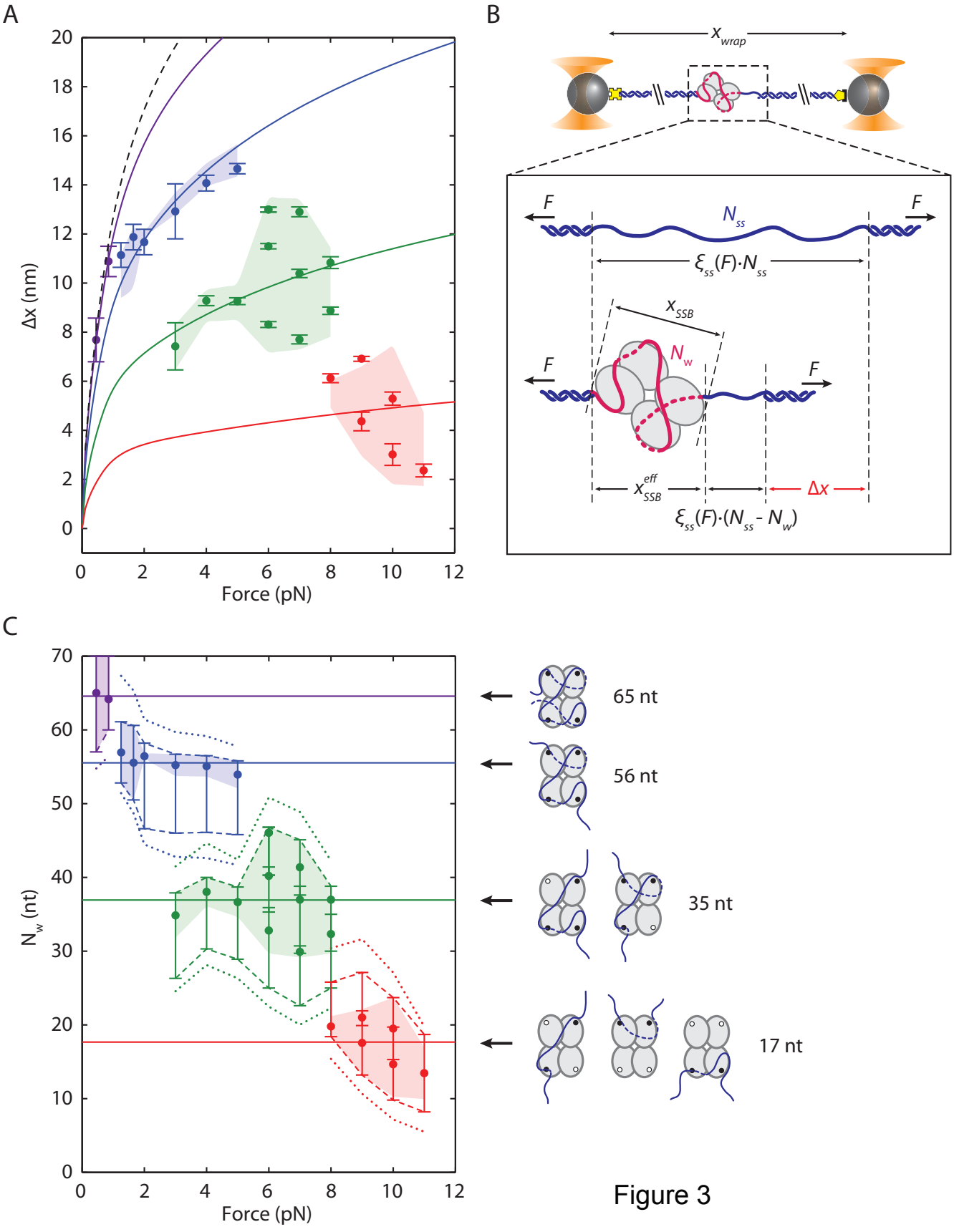
A
Δx (nm)
Force (pN)
B
x_{wrap}
F
N_{ss}
$\xi_{ss}(F)\cdot N_{ss}$
x_{SSB}
N_w
x_{SSB}^{eff}
Δx
$\xi_{ss}(F)\cdot(N_{ss} - N_w)$
C
N_w (nt)
Force (pN)
65 nt
56 nt
35 nt
17 nt

Figure 3

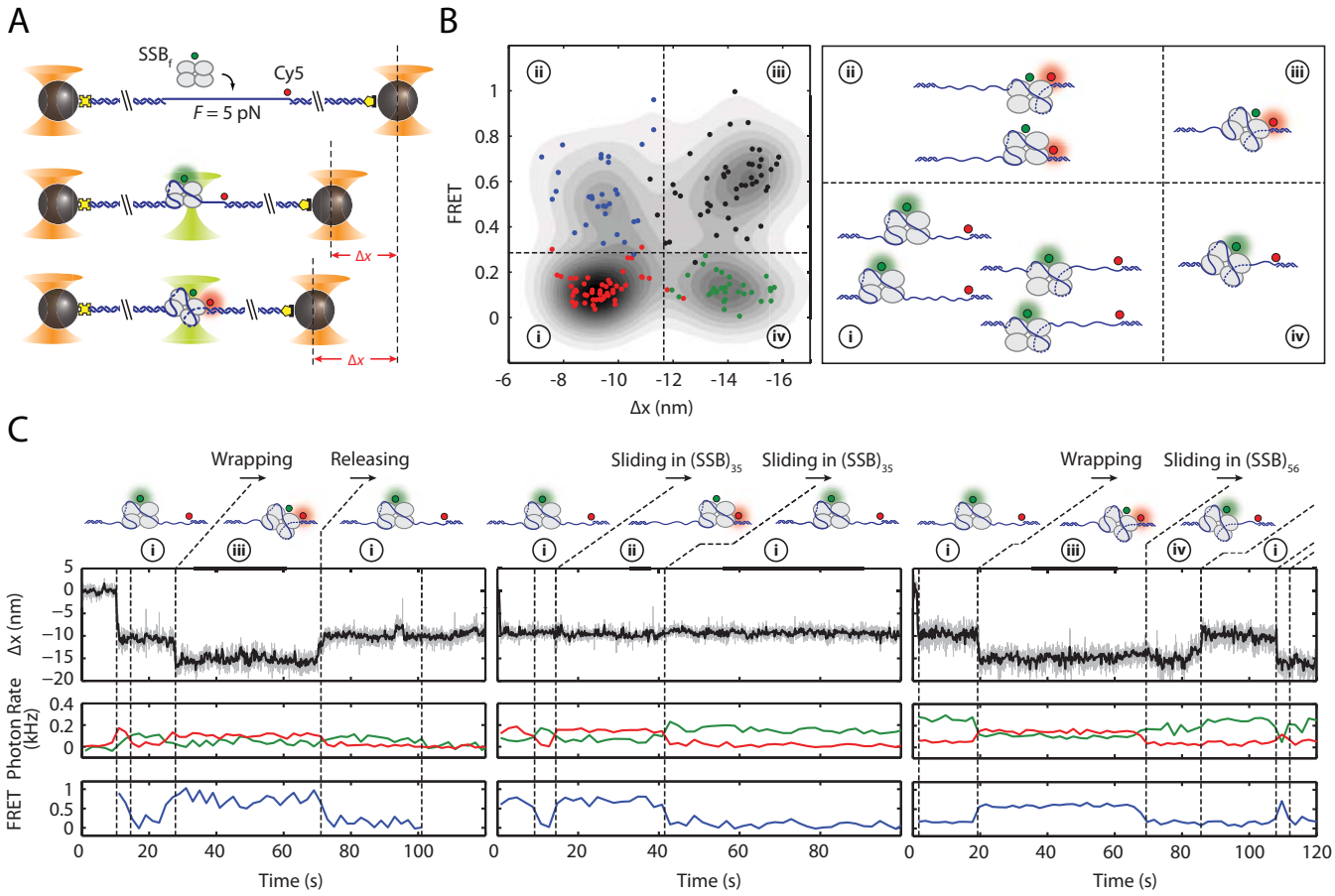
A
SSB
Cy5
F = 5 pN
Δx
Δx
B
FRET
Δx (nm)
C
Wrapping
Releasing
Sliding in (SSB)35
Sliding in (SSB)35
Wrapping
Sliding in (SSB)56
Δx (nm)
Photon Rate (kHz)
FRET
Time (s)
Time (s)
Time (s)

Figure 4

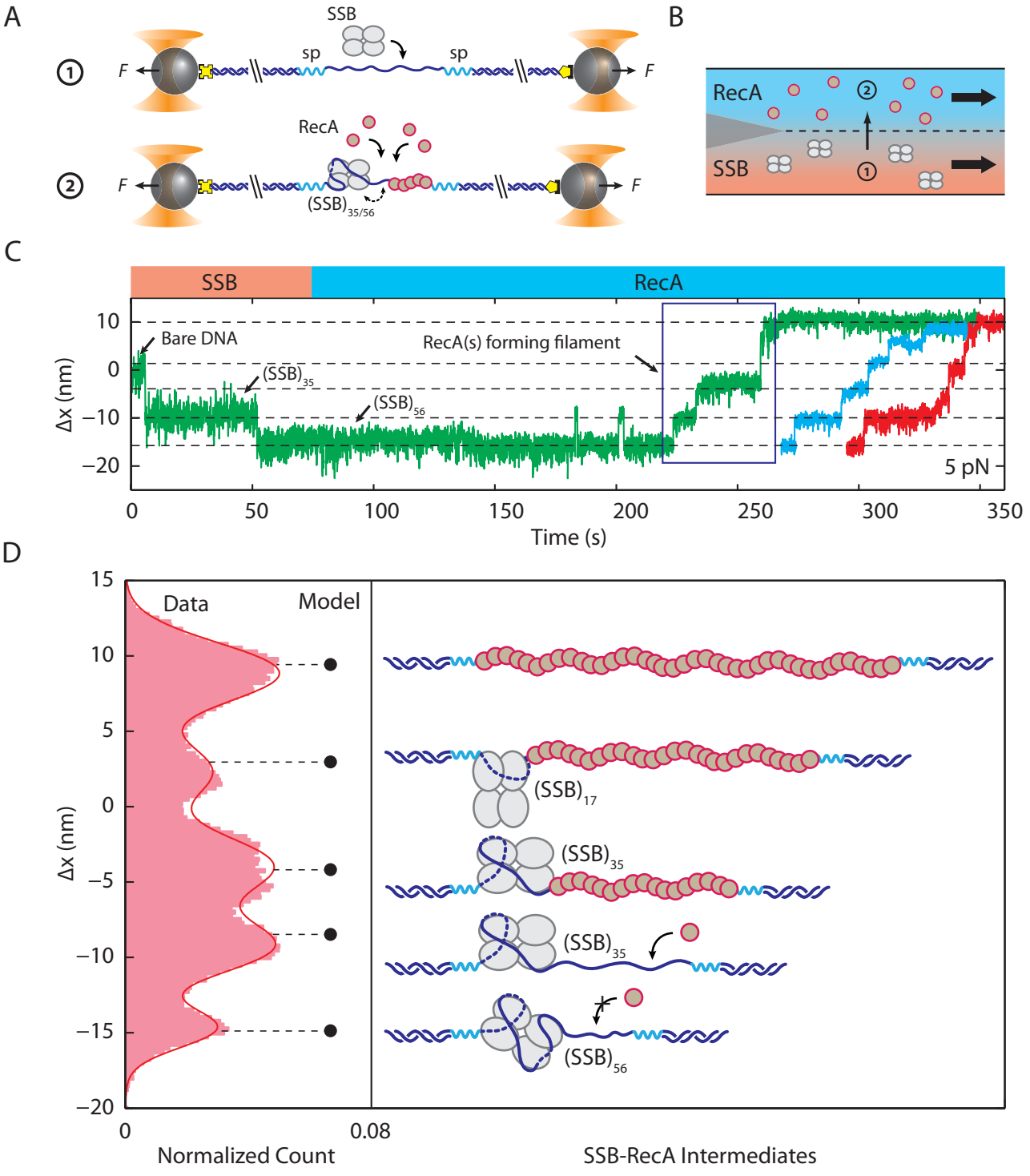
A
SSB
sp
sp
F
F
RecA
(SSB)35/56
B
RecA
SSB
C
SSB
RecA
Bare DNA
RecA(s) forming filament
(SSB)35
(SSB)56
5 pN
Δx (nm)
Time (s)
D
Data
Model
Δx (nm)
Normalized Count
SSB-RecA Intermediates
(SSB)17
(SSB)35
(SSB)35
(SSB)56

Figure 5

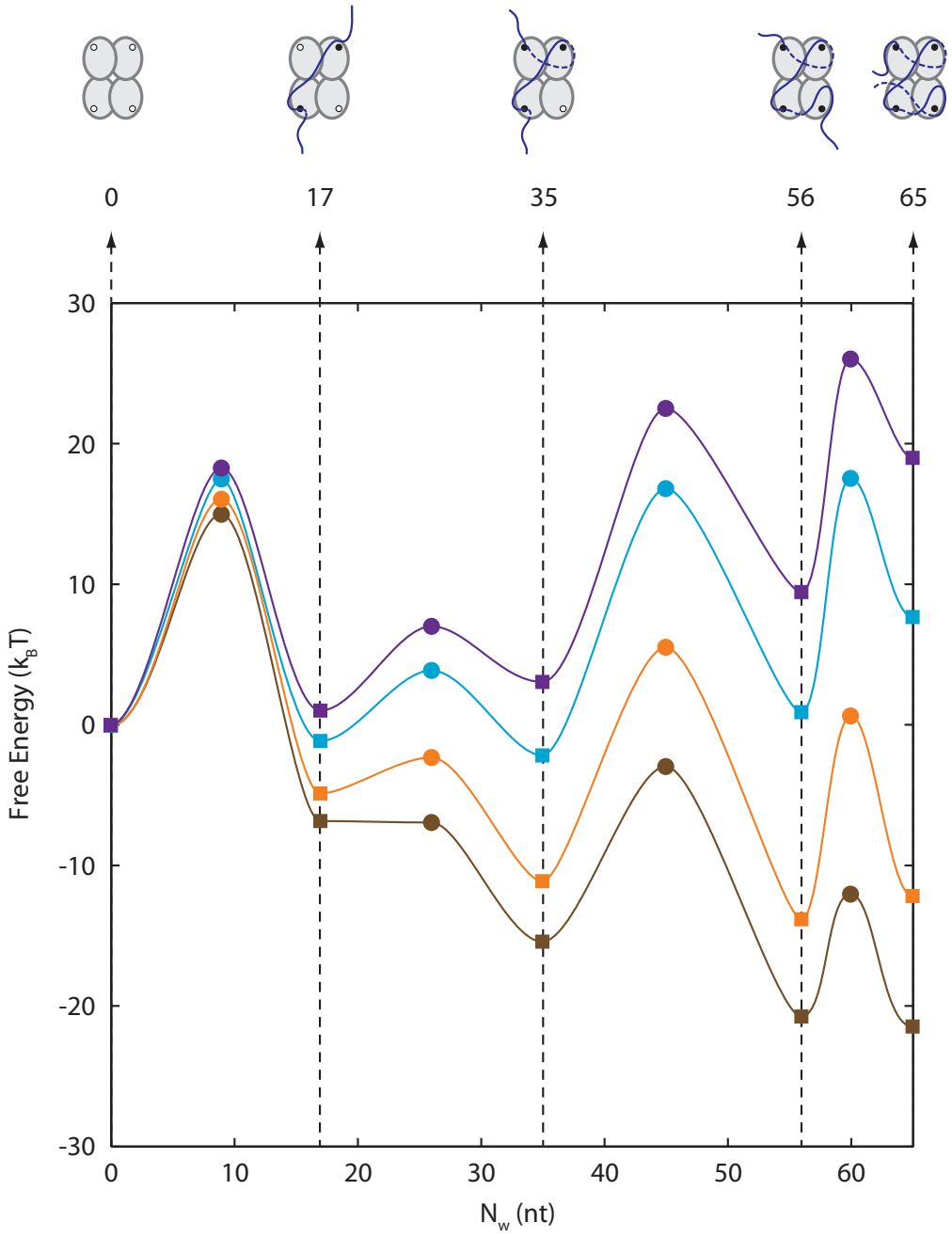
0
17
35
56
65
30
20
10
0
-10
-20
-30
Free Energy (k_BT)
0
10
20
30
40
50
60
N_w (nt)

Figure 6